UMass Chan Medical School

eScholarship@UMassChan

2022-03-11

Innate lymphoid cells and COVID-19 severity in SARS-CoV-2 infection

Noah J. Silverstein
University of Massachusetts Medical School

Et al.

Let us know how access to this document benefits you.

Repository Citation

1

2

Innate lymphoid cells and COVID-19 severity in SARS-CoV-2 infection

4

5

Noah J. Silverstein[1,2,3*], Yetao Wang[1,3*], Zachary Manickas-Hill[3,4], Claudia Carbone[1], Ann Dauphin[1], Brittany P. Boribong[5,6,7], Maggie Loiselle[5], Jameson Davis[5], Maureen M. Leonard[5,6,7], Leticia Kuri-Cervantes[8,9], MGH COVID-19 Collection & Processing Team, Nuala J. Meyer[10], Michael R. Betts[8,9], Jonathan Z. Li[3,11], Bruce Walker[3,4,12,13], Xu G. Yu[3,4,11], Lael M. Yonker[5,6,7], Jeremy Luban[1,3,4,14,15]

[1]Program in Molecular Medicine, University of Massachusetts Medical School, Worcester, MA 01605, USA
[2]Medical Scientist Training Program, University of Massachusetts Medical School, Worcester, MA 01605, USA
[3]Massachusetts Consortium on Pathogen Readiness, Boston, MA, 02115
[4]Ragon Institute of MGH, MIT and Harvard, Cambridge, MA 02139, USA
[5]Massachusetts General Hospital, Mucosal Immunology and Biology Research Center, Boston, MA, USA
[6]Massachusetts General Hospital, Department of Pediatrics, Boston, MA, USA
[7]Harvard Medical School, Boston, MA, USA
[8]Department of Microbiology, Perelman School of Medicine, University of Pennsylvania, Philadelphia, PA 19104, USA
[9]Institute for Immunology, Perelman School of Medicine, University of Pennsylvania, Philadelphia, PA 19104, USA.
[10]Division of Pulmonary and Critical Care Medicine, Department of Medicine, University of Pennsylvania Perelman School of Medicine, Philadelphia, PA 19104, USA
[11]Department of Medicine, Brigham and Women's Hospital, Boston, MA 02115, USA
[12]Howard Hughes Medical Institute, Chevy Chase, MD 20815, USA
[13]Department of Biology and Institute of Medical Engineering and Science, Massachusetts Institute of Technology, Cambridge, MA
[14]Department of Biochemistry and Molecular Biotechnology, University of Massachusetts Medical School, Worcester, MA 01605, USA
[15]Broad Institute of Harvard and MIT, 75 Ames Street, Cambridge, MA 02142, USA

*These authors contributed equally

Correspondence: yetao.wang@umassmed.edu (Y.W.); jeremy.luban@umassmed.edu (J.L.)

Background:
Risk of severe COVID-19 increases with age, is greater in males, and is associated with lymphopenia, but not with higher burden of SARS-CoV-2. It is unknown whether effects of age and sex on abundance of specific lymphoid subsets explain these correlations.

Methods:
Multiple regression was used to determine the relationship between abundance of specific blood lymphoid cell types, age, sex, requirement for hospitalization, duration of hospitalization, and elevation of blood markers of systemic inflammation, in adults hospitalized for severe COVID-19 (n=40), treated for COVID-19 as outpatients (n=51), and in uninfected controls (n=86), as well as in children with COVID-19 (n=19), recovering from COVID-19 (n=14), MIS-C (n=11), recovering from MIS-C (n=7), and pediatric controls (n=17).

Results:
This observational study found that the abundance of innate lymphoid cells (ILCs) decreases more than 7-fold over the human lifespan – T cell subsets decrease less than 2-fold – and is lower in males than in females. After accounting for effects of age and sex, ILCs, but not T cells, were lower in adults hospitalized with COVID-19, independent of lymphopenia. Among SARS-CoV-2-infected adults, the abundance of ILCs, but not of T cells, correlated inversely with odds and duration of hospitalization, and with severity of inflammation. ILCs were also uniquely decreased in pediatric COVID-19 and the numbers of these cells did not recover during follow-up. In contrast, children with MIS-C had depletion of both ILCs and T cells, and both cell types increased during follow-up. In both pediatric COVID-19 and MIS-C, ILC abundance correlated inversely with inflammation. Blood ILC mRNA and phenotype tracked closely with ILCs from lung. Importantly, blood ILCs produced amphiregulin, a protein implicated in disease tolerance and tissue homeostasis. Among controls, the percentage of ILCs that produced amphiregulin was higher in females than in males, and people hospitalized with COVID-19 had a lower percentage of ILCs that produced amphiregulin than did controls.

Conclusions:
These results suggest that, by promoting disease tolerance, homeostatic ILCs decrease morbidity and mortality associated with SARS-CoV-2 infection, and that lower ILC abundance contributes to increased COVID-19 severity with age and in males.

INTRODUCTION

The outcome of SARS-CoV-2 infection is highly variable with only a minority progressing to severe COVID-19, characterized by acute respiratory distress syndrome, multi-organ dysfunction, elevated inflammatory cytokines, lymphopenia, and other abnormalities of the immune system (Bonnet et al., 2021; Giamarellos-Bourboulis et al., 2020; Huang and Pranata, 2020; Kaneko et al., 2020; Kuri-Cervantes et al., 2020; Lucas et al., 2020; Mathew et al., 2020; Mudd et al., 2020; Zhou et al., 2020). The risk of severe COVID-19 and death in people infected with SARS-CoV-2 increases with age and is greater in men than in women (Alkhouli et al., 2020; Bunders and Altfeld, 2020; Gupta et al., 2021; Laxminarayan et al., 2020; Mauvais-Jarvis, 2020; O'Driscoll et al., 2020; Peckham et al., 2020; Richardson et al., 2020; Scully et al., 2020). These trends have been observed in people infected with SARS-CoV (Chen and Subbarao, 2007; Donnelly et al., 2003; Karlberg, 2004), or with MERS-CoV (Alghamdi et al., 2014), and in laboratory animals challenged with SARS-CoV or SARS-CoV-2 (Channappanavar et al., 2017; Leist et al., 2020). The mechanisms underlying these effects of age and sex on COVID-19 morbidity and mortality remain poorly understood.

The composition and function of the human immune system changes with age and exhibits sexual dimorphism (Darboe et al., 2020; Klein and Flanagan, 2016; Márquez et al., 2020; Patin et al., 2018; Solana et al., 2012), with consequences for survival of infection, response to vaccination, and susceptibility to autoimmune disease (Flanagan et al., 2017; Giefing-Kröll et al., 2015; Márquez et al., 2020; Mauvais-Jarvis, 2020; Patin et al., 2018; Piasecka et al., 2018). Better understanding of these effects might provide clues as to why the clinical outcome of SARS-CoV-2 infection is so variable, ranging from

111   asymptomatic to lethal (Cevik et al., 2021; He et al., 2021; Jones et al., 2021; Lee et al.,

112   2020; Lennon et al., 2020; Ra et al., 2021; Richardson et al., 2020; Yang et al., 2021).

113   Survival after infection with a pathogenic virus such as SARS-CoV-2 requires not

114   only that the immune system control and eliminate the pathogen, but that disease

115   tolerance mechanisms limit tissue damage caused by the pathogen or by host

116   inflammatory responses (Ayres, 2020a; McCarville and Ayres, 2018; Medzhitov et al.,

117   2012; Schneider and Ayres, 2008). Research with animal models has demonstrated that

118   genetic and environmental factors can promote host fitness without directly inhibiting

119   pathogen replication (Ayres, 2020a; Cumnock et al., 2018; Jhaveri et al., 2007; McCarville

120   and Ayres, 2018; Medzhitov et al., 2012; Råberg et al., 2007; Sanchez et al., 2018;

121   Schneider and Ayres, 2008; Wang et al., 2016). Although in most cases the underlying

122   mechanism is unknown, some of these models suggest that subsets of innate lymphoid

123   cells (ILCs) contribute to disease tolerance (Artis and Spits, 2015; Branzk et al., 2018;

124   Califano et al., 2018; Diefenbach et al., 2020; McCarville and Ayres, 2018; Monticelli et

125   al., 2015, 2011). Some ILC subsets produce the epidermal growth factor family member

126   amphiregulin (AREG) that maintains the integrity of epithelial barriers in the lung and

127   intestine (Branzk et al., 2018; Jamieson et al., 2013; Monticelli et al., 2015, 2011), and

128   promotes tissue repair (Artis and Spits, 2015; Cherrier et al., 2018; Klose and Artis, 2016;

129   Rak et al., 2016). In models of influenza infection in mice, homeostatic ILCs and

130   exogenous AREG promote lung epithelial integrity, decrease disease severity, and

131   increase survival, without decreasing pathogen burden (Califano et al., 2018; Jamieson

132   et al., 2013; Monticelli et al., 2011).

133   Little is known about disease tolerance in the context of human infectious

134   diseases. Interestingly, SARS-CoV-2 viral load does not reliably discriminate

135   symptomatic from asymptomatic infection (Cevik et al., 2021; Jones et al., 2021; Lee et

136   al., 2020; Lennon et al., 2021; Ra et al., 2021; Yang et al., 2021). This discrepancy

137   between SARS-CoV-2 viral load and the severity of COVID-19 is especially pronounced

138   in children, who rarely have severe COVID-19 (Charles Bailey et al., 2020; Li et al., 2020;

139   Lu et al., 2020; Poline et al., 2020), though viral load may be comparable to that in adults

140   with severe COVID-19 (Heald-Sargent et al., 2020; LoTempio et al., 2021; Yonker et al.,

141   2020). These observations suggest that age-dependent, disease tolerance mechanisms

142   influence the severity of COVID-19. In mice, homeostatic ILCs decrease in abundance in

143   the lung with increasing age, and lose their ability to maintain disease tolerance during

144   influenza infection (D'Souza et al., 2019). Although the distribution of ILCs within human

145   tissues differs from mice and is heterogeneous among individuals (Yudanin et al., 2019),

146   human ILCs share many features with those in mice (Vivier et al., 2018) and therefore

147   may perform similar roles in maintaining tissue homeostasis and disease tolerance.

148   ILCs in peripheral blood have been reported to be depleted in individuals with

149   severe COVID-19 (García et al., 2020; Kuri-Cervantes et al., 2020), but it is difficult to

150   determine the extent to which ILCs are decreased independently from the overall

151   lymphopenia associated with COVID-19 (Chen et al., 2020; Huang et al., 2020; Huang

152   and Pranata, 2020; Zhang et al., 2020; Zhao et al., 2020), or from changes in other blood

153   cell lineages (Giamarellos-Bourboulis et al., 2020; Huang et al., 2020; Kuri-Cervantes et

154   al., 2020; Lucas et al., 2020; Mathew et al., 2020; Mudd et al., 2020; Zheng et al., 2020).

155   In addition, assessment of lymphoid cell abundance, in the context of a disease for which

156   age and sex are risk factors for severity, is confounded by programmed differences in

157   lymphocyte abundance with age and sex (Márquez et al., 2020; Patin et al., 2018). The

158   goal of this study was to determine whether the abundance of any blood lymphoid cell

159   population was altered in COVID-19, independent of age, sex, and global lymphopenia,

160   and whether abundance of any lymphoid cell population correlated with clinical outcome

161   in SARS-CoV-2 infection.

162 **Materials and Methods**

Key Resources Table				
Reagent type (species) or resource	Designation	Source or reference	Identifiers	Additional information
antibody	Anti-Human BDCA1 (mouse monoclonal)	Biolegend	Cat# 354208	Clone: 201A (FITC) (1:200 dilution)
antibody	Anti-Human CD117 (mouse monoclonal)	Biolegend	Cat# 313206	Clone: 104D2 (APC) (1:200 dilution)
antibody	Anti-Human CD11c (mouse monoclonal)	Biolegend	Cat# 301604	Clone: 3.9 (FITC) (1:200 dilution)
antibody	Anti-Human CD123 (mouse monoclonal)	Biolegend	Cat# 306014	Clone: 6H6 (FITC) (1:200 dilution)
antibody	Anti-Human CD127 (mouse monoclonal)	Biolegend	Cat# 351320	Clone: A019D5 (PE/Cyanine7) (1:200 dilution)
antibody	Anti-Human CD14 (mouse monoclonal)	Biolegend	Cat# 325604	Clone: HCD14 (FITC) (1:200 dilution)
antibody	Anti-Human CD16 (mouse monoclonal)	Biolegend	Cat# 980104	Clone: 3G8 (APC) (1:400 diltuion)
antibody	Anti-Human CD19 (mouse monoclonal)	Biolegend	Cat# 302206	Clone: HIB19 (FITC) (1:200 dilution)

antibody	Anti-Human CD1a (mouse monoclonal)	Biolegend	Cat# 300104	Clone: HI149 (FITC) (1:200 dilution)
antibody	Anti-Human CD20 (mouse monoclonal)	Biolegend	Cat# 302304	Clone: 2H7a (FITC) (1:200 dilution)
antibody	Anti-Human CD22 (mouse monoclonal)	Biolegend	Cat# 363508	Clone: S-HCL-1 (FITC) (1:200 dilution)
antibody	Anti-Human CD3 (mouse monoclonal)	Biolegend	Cat# 317306	Clone: OKT3 (FITC) (1:200 dilution)
antibody	Anti-Human CD34 (mouse monoclonal)	Biolegend	Cat# 343504	Clone: 581 (FITC) (1:200 dilution)
antibody	Anti-Human CD4 (mouse monoclonal)	Biolegend	Cat# 317428	Clone: OKT4 (PerCP/Cyanine5.5) (1:200 dilution)
antibody	Anti-Human CD4 (mouse monoclonal)	Biolegend	Cat# 317408	Clone: OKT4 (FITC) (1:200 dilution)
antibody	Anti-Human CD45 (mouse monoclonal)	BD	Cat# 560178	Clone: 2D1 (APC/H7) (1:200 diltuion)
antibody	Anti-Human CD56 (mouse monoclonal)	Biolegend	Cat# 318306	Clone: HCD56 (PE) (1:200 dilution)
antibody	Anti-Human CD8 (mouse monoclonal)	Biolegend	Cat# 300924	Clone: HIT8a (PerCP/Cyanine 5.5) (1:200 dilution)

antibody	Anti-Human CRTH2 (rat monoclonal)	Biolegend	Cat# 350116	Clone: BM16 (PerCP/Cyanine5.5) (1:200 dilution)
antibody	Anti-Human FcεR1α (mouse monoclonal)	Biolegend	Cat# 334608	Clone: AER-37 (FITC) (1:200 dilution)
antibody	Anti-Human TBX21 (mouse monoclonal)	ebioscience	Cat# 25-5825-82	Clone: ebio4B10 (PE/Cyanine7) (1:200 dilution)
antibody	Anti-Human TCRα/β (mouse monoclonal)	Biolegend	Cat# 306706	Clone: IP26 (FITC) (1:200 dilution)
antibody	Anti-Human TCRγ/δ (mouse monoclonal)	Biolegend	Cat# 331208	Clone: B1 (FITC) (1:200 dilution)
antibody	Anti-Human TCF7 (rabbit monoclonal)	Cell Signaling	Cat# 37636s	Clone: C63D9 (APC) (1:200 dilution)
antibody	Anti-Human IL-13 (rat monoclonal)	Biolegend	Cat# 501908	Clone: JES10-5A2 (APC) (1:200 dilution)
antibody	Anti-Human AREG (mouse monoclonal)	ebioscience	Cat# 17-5370-42	Clone: AREG559
antibody	mouse IgG1, k isotype control (mouse monoclonal)	Biolegend	Cat# 400112	Clone: MOPC-21 (PE) (1:200 dilution)
antibody	mouse IgG1, k isotype control	Biolegend	Cat# 400120	Clone: MOPC-21 (APC) (1:200 dilution)

	(mouse monoclonal)			
antibody	Rabbit IgG, isotype control (rabbit monoclonal)	Cell Signaling	Cat# 3452S	(Alexa Fluor 647) (1:200 dilution)
antibody	Rat IgG1, k isotype control (rat monoclonal)	Biolegend	Cat# 400412	Clone: RTK2071 (APC) (1:200 dilution)
Biological Samples (Homo sapiens)	PBMCs	New York Biologics	https://www.newyorkbiologics.com/	
Biological Samples (Homo sapiens)	PBMCs	MassCPR	https://masscpr.hms.harvard.edu/	
Biological Samples (Homo sapiens)	PBMCs	MGH Pediatric COVID-19 Biorepository		
commercial assay or kit	cell stimulation cocktail	eBioscience	Cat# 00-4970-03	
chemical compound, drug	protein transport inhibitor	eBioscience	Cat# 00-4980-03	
chemical compound, drug	TRIzol reagent	Invitrogen	Cat# 15596018	
commercial assay or kit	AMPure XP beads	Beckman Culter	Cat# A63880	
commercial assay or kit	ExoSAP-IT	Affymetrix	Cat# 78200	

commercial assay or kit	Live and Dead violet viability kit	Invitrogen	Cat# L-34963	
commercial assay or kit	Foxp3 / Transcription Factor Staining Buffer Set	eBioscience	Cat# 00-5523-00	
commercial assay or kit	HiScribe T7 High Yield RNA Synthesis Kit	NEB	Cat# E2040S	
commercial assay or kit	NEBNext Ultra II Non directional Second Strand Synthesis Module	NEB	Cat# E6111L	
software, algorithm	R computer software environment (version 4.0.2)	The R Foundation (R Core Team, 2020)	https://www.r-project.org/	
software, algorithm	FlowJo	FlowJo, LLC	https://www.flowjo.com/	
software, algorithm	tidyverse v1.3.1	(Wickham et al., 2019)	https://www.tidyverse.org	
software, algorithm	ggplot2 v3.3.3	(Wickham, 2016)	https://ggplot2.tidyverse.org	
software, algorithm	ggpubr v0.4.0	(Kassambara, 2020)	https://rpkgs.datanovia.com/ggpubr/	
software, algorithm	ComplexHeatmap v2.4.3	(Gu et al., 2016)	https://github.com/jokergoo/ComplexHeatmap	
software, algorithm	emmeans v1.6.0	(Lenth, 2020)	https://CRAN.R-project.org/package=emmeans	

software, algorithm	lme4 v1.1-27	(Bates et al., 2015)	https://cran.r-project.org/web/packages/lme4/index.html	
software, algorithm	lmerTest v3.1-3	(Kuznetsova et al., 2017)	https://cran.r-project.org/web/packages/lmerTest/index.html	
software, algorithm	DolphinNext RNA-seq pipeline (Revision 4)	(Yukselen et al., 2020)	https://github.com/UMMS-Biocore/dolphinnext	
software, algorithm	STAR v2.1.6	(Dobin et al., 2013)	https://github.com/alexdobin/STAR	
software, algorithm	RSEM v1.3.1	(Li and Dewey, 2011)	http://deweylab.github.io/RSEM/	
software, algorithm	DEseq2 v1.28.1	(Love et al., 2014)	https://bioconductor.org/packages/release/bioc/html/DESeq2.html	
software, algorithm	clusterProfiler v3.16.1	(Yu et al., 2012)	https://guangchuangyu.github.io/software/clusterProfiler/	

163

Peripheral blood PBMCs

164

165 As part of a COVID-19 observational study, peripheral blood samples were collected

166 between March 31st and June 3rd of 2020 from 91 adults with SARS-CoV-2 infection,

167 either after admission to Massachusetts General Hospital for the hospitalized cohort, or

168 while at affiliated outpatient clinics for the outpatient cohort. Request for access to coded

169 patient samples was reviewed by the Massachusetts Consortium for Pathogen Readiness

170 (https://masscpr.hms.harvard.edu/) and approved by the University of Massachusetts

171 Medical School IRB (protocol #H00020836). Pediatric participants with COVID-19 or MIS-

172 C were enrolled in the Massachusetts General Hospital Pediatric COVID-19 Biorepository

173 (MGB IRB # 2020P000955). Healthy pediatric controls were enrolled in the Pediatric

174   Biorepository (MGB IRB # 2016P000949). Samples were collected after obtaining

175   consent from the patient if 18 years or older, or from the parent/guardian, plus assent

176   when appropriate. Demographic, laboratory, and clinical outcome data were included with

177   the coded samples. Samples from 86 adult blood donors and 17 pediatric blood donors

178   were included as controls; these were either collected prior to the SARS-CoV-2 outbreak

179   or from healthy individuals screened at a blood bank.

180

181   **Human mononuclear cell isolation**

182   Human peripheral blood was diluted in an equal volume of RPMI-1640 (Gibco), overlaid

183   on Lymphoprep (STEMCELL Technologies, #07851), and centrifuged at 500 x g at room

184   temperature for 30 minutes. Mononuclear cells were washed 3 times with MACS buffer

185   (0.5% BSA and 2 mM EDTA in PBS) and frozen in FBS containing 10% DMSO.

186
187   **Flow cytometry**

188   Peripheral blood mononuclear cells (PBMCs) were first stained with Live and Dead violet

189   viability kit (Invitrogen, L-34963). To detect surface molecules, cells were stained in

190   MACS buffer with antibodies (Supplementary file 1a) for 30 min at 4°C in the dark. To

191   detect IL-13 or AREG, cells were stimulated with PMA and ionomycin (eBioscience, 00-

192   4970-03) for 3 hours with Brefeldin A and Monensin (eBioscience, 00-4980-03) present

193   during the stimulation. To detect transcription factors or cytokines, cells were fixed and

194   permeabilized using Foxp3 staining buffer kit (eBioscience, 00-5523-00), then

195   intracellular molecules were stained in permeabilization buffer with antibodies. Cells were

196   detected on a BD Celesta flow cytometer using previously established gating strategies

197   (Wang et al., 2020). Cell subsets were identified using FlowJo™ software (Becton,

198   Dickson and Company). Representative gating strategies are shown in Figure 2–figure

199   supplement 1.

200   **Bulk RNA-Seq Library preparation of PBMC ILCs**

201   The sequencing libraries were prepared using CEL-Seq2 (Hashimshony et al., 2016).

202   RNA from sorted cells was extracted using TRIzol reagent (ThermoFisher, 15596018).

203   10 ng RNA was used for first strand cDNA synthesis using barcoded primers (the specific

204   primers for each sample were listed in Supplementary file 1b). The second strand was

205   synthesized by NEBNext Second Strand Synthesis Module (NEB, E6111L). The pooled

206   dsDNA was purified with AMPure XP beads (Beckman Coulter, A63880), and subjected

207   to in vitro transcription (IVT) using HiScribe T7 High Yield RNA Synthesis Kit (NEB,

208   E2040S), then treated with ExoSAP-IT (Affymetrix, 78200). IVT RNA was fragmented

209   using RNA fragmentation reagents (Ambion) and underwent another reverse transcription

210   step using random hexamer RT primer-5'-GCC TTG GCA CCC GAG AAT TCC ANN NNN

211   N-3' to incorporate the second adapter. The final library was amplified with indexed

212   primers: RP1 and RPI1 (Supplementary file 1b), and the bead purified library was

213   quantified with 4200 TapeStation (Agilent Technologies) and paired end sequenced on

214   Nextseq 500 V2 (Illumina), Read 1: 15 cycles; index 1: 6 cycles; Read 2: 60 cycles.

215

216   **RNA-seq analyses**

217   Pooled reads from PBMC-derived ILCs were separated by CEL-Seq2 barcodes, and

218   demultiplexed reads from RNA-seq of ILCs from lung (Ardain et al., 2019), spleen, and

219   intestine (Yudanin et al., 2019), were downloaded from GSE131031 and GSE126107.

220   Within the DolphinNext RNA-seq pipeline (Revision 4) (Yukselen et al., 2020), reads were

221 aligned to the hg19 genome using STAR (version 2.1.6)(Dobin et al., 2013) and counts

222 of reads aligned to RefSeq genes were quantified using RSEM (version 1.3.1)(Li and

223 Dewey, 2011). Normalized transcript abundance in the form of TPMs were used to filter

224 out low abundance transcripts with an average of <3 TPMs across libraries. RSEM-

225 generated expected counts were normalized and differential analysis was performed

226 using DEseq2 (Love et al., 2014) in R, with significant genes defined as a greater than

227 1.5-fold difference and an adjusted p-value <0.01. GO Enrichment Analysis was

228 performed in R using the enrichGO function in the clusterProfiler R package (Yu et al.,

229 2012). Data were transformed using vsd within DEseq2 both for the heatmap visualization

230 with ComplexHeatmap (Gu et al., 2016) and for principal component analysis (PCA) with

231 prcomp on the top 250 most variable genes. Normalized counts were generated for

232 plotting using the counts command in Deseq2.

233

234 **Statistical analysis and data visualization**

235 Data were prepared for analysis with tidyverse packages (Wickham et al., 2019) and

236 visualized using the ggplot2 (Wickham, 2016), ggpubr (Kassambara, 2020), and

237 ComplexHeatmap (Gu et al., 2016) packages, within the R computer software

238 environment (version 4.0.2) (R Core Team, 2020). Group differences were determined

239 with pairwise, two-sided, Wilcoxon rank-sum tests, or Fisher's exact test, as indicated,

240 with Bonferroni correction for multiple comparisons. Multiple linear regression analyses

241 were performed with dependent and independent variables as indicated in the text, using

242 the lm function in R. Pairwise group comparisons on estimated marginal means

243 generated from multiple linear regression were performed using the emmeans package

244 (Lenth, 2020) in R, with multiple comparison correction using the Tukey adjustment.

245   Multiple logistic regressions were performed using the glm function in R. Longitudinal

246   follow-up analyses on pediatric COVID-19 and MIS-C was performed with linear mixed-

247   effect models using lme4 (Bates et al., 2015) in R with the equation: log2 (lymphoid cell

248   abundance) ~ Age + Sex + Group + Group:Follow_up + (1|Patient_ID). This model tested

249   the effect of followup on ILC abundance in the pediatric COVID-19 and MIS-C groups

250   while accounting for age, sex, and group. Statistical significance was determined with

251   lmerTest (Kuznetsova et al., 2017) in R, using the Satterthwarte's degrees of freedom

252   method. $p < 0.05$ was considered significant. United States SARS-CoV-2 infection and

253   mortality data were downloaded from (CDC Case Surveillance Task Force, 2020) and

254   cases with age group and outcome available were plotted by age group as indicated.

255   Mortality rate was calculated by dividing the number of fatal cases by the total number of

256   cases with known outcome in each age group as indicated.

257   **Data availability**

258   The data that support the findings of this study are available within the manuscript and in

259   its supplementary information data files. Bulk RNA-seq datasets generated here can be

260   found at: NCBI Gene Expression Omnibus (GEO): GSE168212. Bulk RNA-seq data

261   generated by previously published studies are available from NCBI GEO: GSE131031

262   and GSE126107. This study did not generate unique code.

263

264

RESULTS

Characteristics of adult blood donors hospitalized for COVID-19, treated for COVID-19 as outpatients, or SARS-CoV-2-uninfected controls

The first group of blood donors in this study included SARS-CoV-2-infected adults hospitalized for severe COVID-19 (N = 40), among whom 33 (82.5%) were admitted to the ICU, 32 (80%) required intubation with mechanical ventilation, and 7 (17.5%) died (Table 1). Aside from intubation, information regarding treatment during hospitalization was not available. This group had a mean age of 57.6 (range 24 to 83) and 60% were males. The second group consisted of adults infected with SARS-CoV-2 who were treated for COVID-19 as outpatients (N=51). This group had a mean age of 36.8 years (range 23-77) and was 25.5% male (Table 1). Differences between these two SARS-CoV-2-infected groups, in terms of median age ($p = 5.2 \times 10^{-8}$), sex ratio ($p = 3.7 \times 10^{-3}$), and diagnosis of diabetes mellitus ($p = 1.05 \times 10^{-3}$), were consistent with established risk factors for severe COVID-19 (Fig. 1 and Table 1) (Alkhouli et al., 2020; Bunders and Altfeld, 2020; Gupta et al., 2021; Laxminarayan et al., 2020; Mauvais-Jarvis, 2020; O'Driscoll et al., 2020; Peckham et al., 2020; Petrilli et al., 2020; Richardson et al., 2020; Scully et al., 2020). Available information concerning ethnicity and race of the blood donors was insufficient for statistical comparisons among the groups (Supplementary file 2a). Finally, 86 adults who donated blood prior to the SARS-CoV-2 outbreak, or who were screened at a blood donation center, were included as controls for SARS-CoV-2 infection. The age of this group spanned the range of the two groups of SARS-CoV-2-infected people (mean age 50.9; range 23 to 79), and the percentage of males (55.8%) was similar to that of the group hospitalized for COVID-19 (Table 1 and Fig. 1). Complete information

regarding ethnicity, race, and comorbidity was not available for control blood donors.

289

Table 1: Demographic and Clinical Characteristics of Adult Blood Donor Groups

| Characteristic	Control N=86	Hospitalized N=40	Outpatient N=51
Mean age (range) - years	50.9 (23-79)	57.6 (24-83)	36.8 (23-77)
Sex – number (%)			
Male	48 (55.8)	24 (60)	13 (25.5)
Female	38 (44.2)	16 (40)	38 (74.5)
Mean symptom duration at sample collection (range) – days		21.8 (5-66)	26.9 (1-61)
Diabetes mellitus diagnosis – number (%)		11 (27.5)	1 (2)
ICU admission – number (%)		33 (82.5)	
Intubation with mechanical ventilation – number (%)		32 (80)	
Deaths – number (%)		7 (17.5)	
Mean time hospitalized (range) – days		34.2 (4-87)	
Max lab value – mean (range)			
CRP – mg/L		228.6 (6.5-539.5)	
ESR – mm/h		89.0 (15-146)	
D-dimer – (ng/mL)		5700 (351-11923)	

290

291

Characteristics of pediatric blood donors with COVID-19, MIS-C, or SARS-CoV-2-uninfected controls

Children are less likely than adults to have severe disease when infected with SARS-CoV-2 despite having viral loads as high as adults (Charles Bailey et al., 2020; Heald-Sargent et al., 2020; Li et al., 2020; LoTempio et al., 2021; Lu et al., 2020; Poline et al., 2020; Yonker et al., 2020). Rarely, after SARS-CoV-2 clearance from the upper airways, children can develop severe Multisystem Inflammatory Syndrome in Children (MIS-C), a life-threatening condition distinct from COVID-19 that presents with high fevers and multiorgan injury, often including coronary aneurysms, ventricular failure, or myocarditis (Cheung et al., 2020; Feldstein et al., 2021, 2020; Licciardi et al., 2020; Riphagen et al., 2020; Verdoni et al., 2020; Whittaker et al., 2020).

The first cohort of pediatric blood donors in this study consisted of patients with COVID-19 who were treated in hospital (N=11) or as outpatients (N=8). The second cohort of pediatric blood donors was patients hospitalized for MIS-C (N=11). Seventeen SARS-CoV-2-uninfected pediatric blood donors constituted a control group. No significant differences in age or percentage of males were detected among the pediatric COVID-19, MIS-C, or pediatric control groups (Supplementary file 2b and Fig. 1).

311
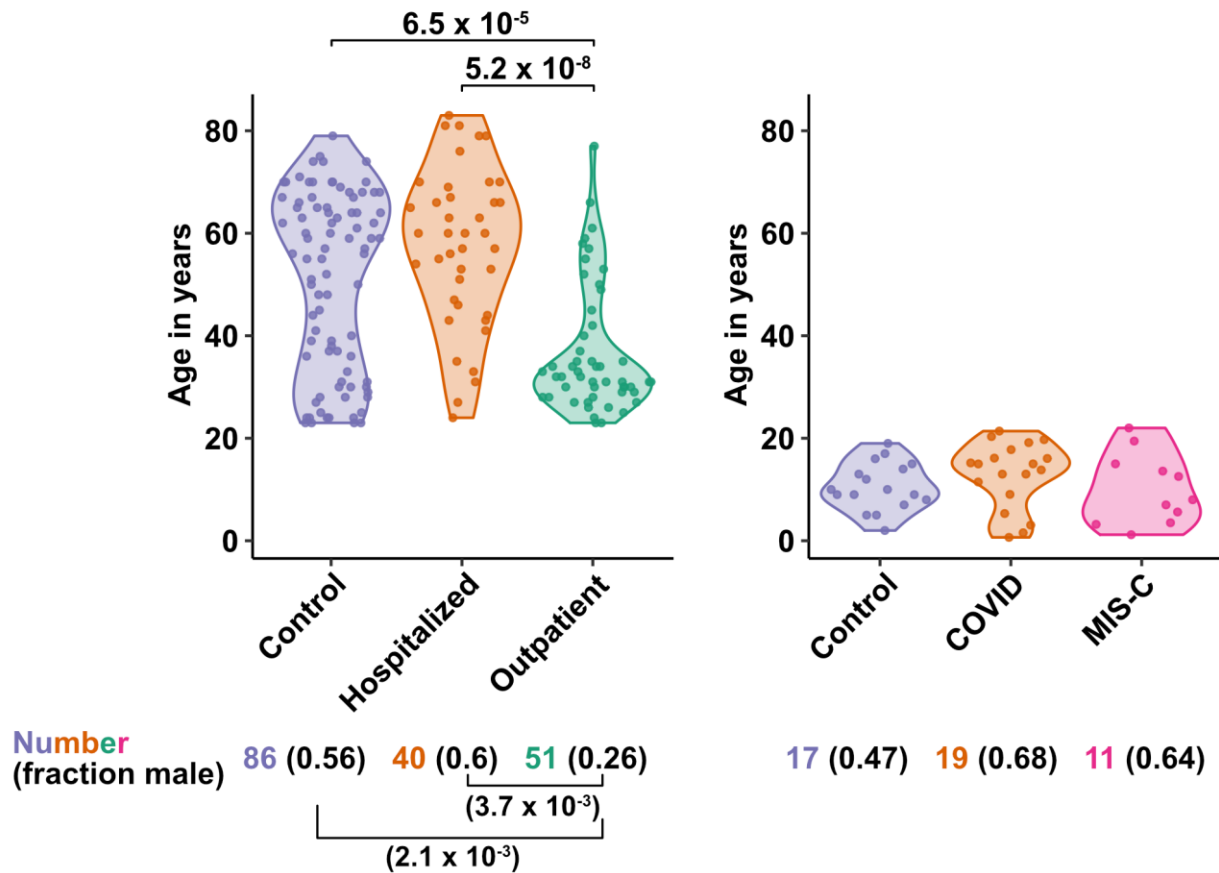
Fig. 1. Age and sex of control and SARS-CoV-2-infected blood donors

Age of the subjects is shown, along with the number of subjects and fraction male in each group, for adult (left) and pediatric (right) cohorts, as indicated. P-values are from pairwise, two-sided, Wilcoxon rank-sum test for ages and Fisher's exact test for fraction male, with Bonferroni correction for multiple comparisons. Adjusted P-values < 0.05 are shown.

318

319

Blood ILC abundance decreases exponentially across the lifespan and is sexually dimorphic

Lymphoid cell abundance in peripheral blood changes with age and is sexually dimorphic (Márquez et al., 2020; Patin et al., 2018). Previous studies reporting the effect of COVID-19 on the abundance of blood lymphoid cell subsets have not fully accounted for the association of age and sex with COVID-19 severity. To isolate the effect of COVID-19 on cell abundance from effects of age and sex, PBMCs were collected from 103 SARS-CoV-2-negative blood donors distributed from 2 to 79 years of age, with a nearly equal ratio of males to females (Supplementary file 2c). Abundance of lymphoid cell types was plotted by 20-year age groups (Fig. 2A), as well as by sex (Fig. 2B). Lymphoid cell types assessed here included CD4$^+$ T cells, CD8$^+$ T cells, ILCs, and FcγRIII (CD16)-positive NK cells. Like CD8$^+$ T cells, NK cells kill virus-infected cells using perforin and granzyme (Artis and Spits, 2015; Cherrier et al., 2018). Additionally, by binding virus-specific immunoglobulins that target virus-infected cells for antibody-dependent cellular cytotoxicity, CD16$^+$ NK cells link innate and acquired immunity (Anegon et al., 1988).

All cell types examined here were affected by age, but ILCs were the only subset with significant differences among all age groups, falling approximately 2-fold in median abundance every 20 years, with a greater than 7-fold decrease from the youngest to oldest age groups ($p = 1.64 \times 10^{-11}$) (Fig. 2A). This magnitude decrease was unique to ILCs and corresponded inversely with the exponential increase in COVID-19 mortality with age (O'Driscoll et al., 2020) (Fig. 2C). In addition, both ILCs and CD4$^+$ T cells were less abundant in males (Fig. 2B). These findings highlight the importance of accounting for effects of age and sex when assessing group differences in lymphoid cell abundance,

21

343   particularly in the context of a disease such as COVID-19 that disproportionately affects

344   older males (O'Driscoll et al., 2020).

345

346
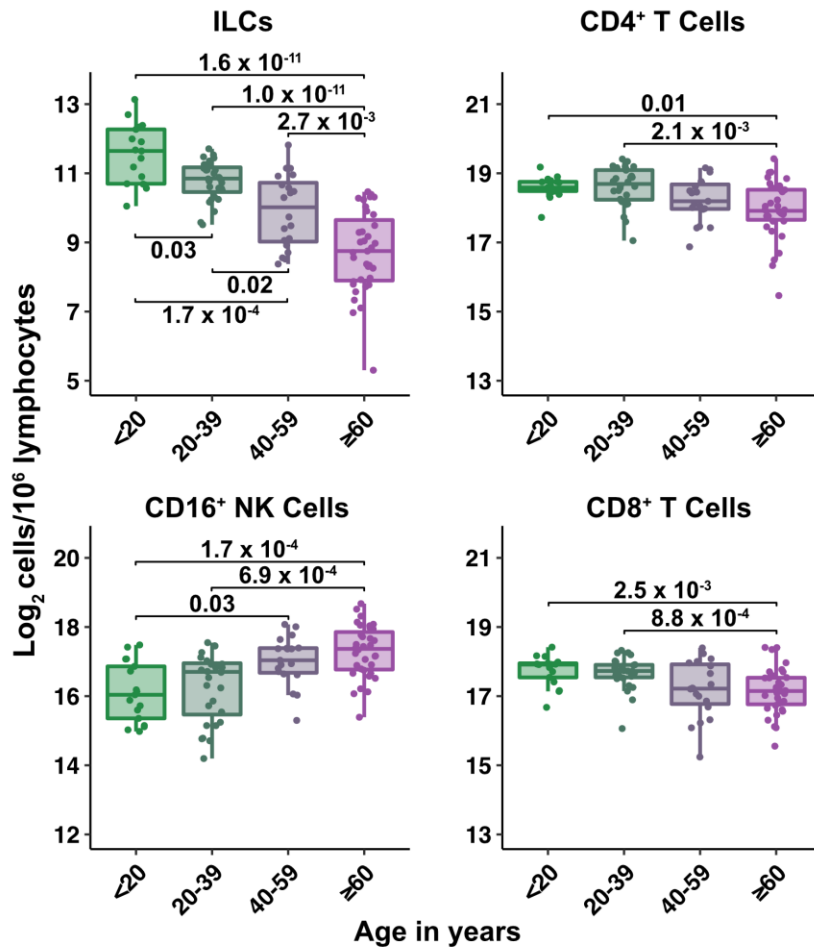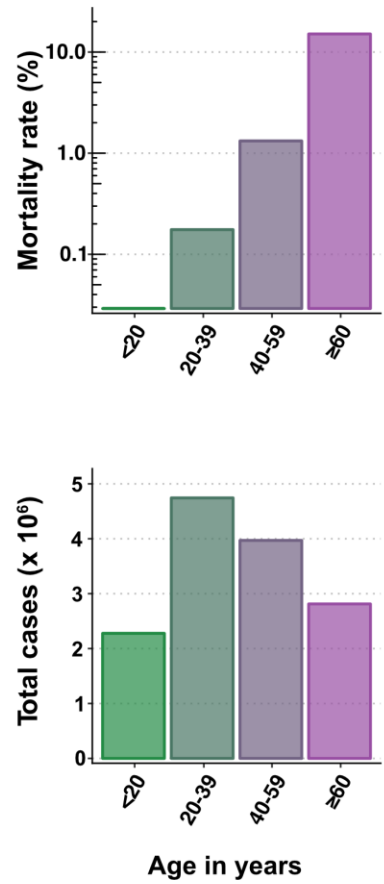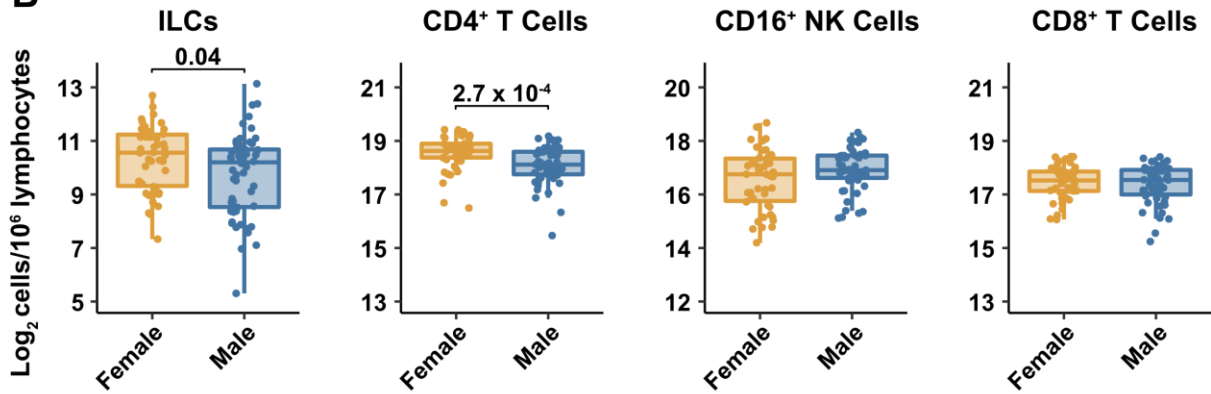
Fig. 2. Blood ILC abundance decreases exponentially across the lifespan mirroring the mortality rate from SARS-CoV-2 infection

349   (**A-B**) Log2 abundance per million lymphocytes of the indicated lymphoid cell populations

350   in combined pediatric and adult control data plotted by 20-year bin or by sex, as indicated.

351   Each dot represents an individual blood donor. Boxplots represent the distribution of the

352   data with the center line drawn through the median with the upper and lower bounds of

353   the box at the 75th and 25th percentiles respectively. The upper and lower whiskers

354   extend to the largest or smallest values within 1.5 x the interquartile range (IQR). P-values

355   are from two-sided, Wilcoxon rank-sum tests with Bonferroni correction for multiple

356   comparisons. Adjusted P-values < 0.05 are shown.

357   (**C**) Case numbers and mortality rate within the indicated age ranges for cases reported

358   in the United States between Jan 1, 2020, and June 6, 2021.

359

360

361

362

363

364

365

366

367

368

369

370

371

Adults hospitalized with COVID-19 have fewer total lymphocytes even after accounting for effects of age and sex

Severe COVID-19 is associated with lymphopenia (Chen et al., 2020; Huang et al., 2020; Huang and Pranata, 2020; Zhang et al., 2020; Zhao et al., 2020) but it remains unclear if this effect is due to reduction in particular lymphoid cell subpopulations, or whether this effect is explained by the more advanced age and higher proportion of males among people with severe COVID-19. As a first step to assess the specificity of lymphocyte depletion, the effect of COVID-19 on total lymphocyte abundance was addressed with multiple linear regression. After accounting for effects of age and sex, individuals hospitalized with severe COVID-19 had 1.33-fold (95%CI: 1.49–1.19; p = 1.22 x 10^{-6}) fewer total lymphocytes among PBMCs than did controls (Supplementary file 2d). Lymphocyte abundance in people infected with SARS-CoV-2 who were treated as outpatients was not different from controls (Supplementary file 2d). In addition, total lymphocytes decreased with age and were less abundant in males (Supplementary file 2d). Subsequent analyses of lymphoid cell subsets took into account the depletion in total lymphocytes associated with COVID-19 by assessing lymphoid subsets as a fraction of total lymphocytes.

After accounting for age and sex, only innate lymphoid cells are depleted in severe COVID-19

To determine whether there were independent associations between lymphoid cell subsets and COVID-19, multiple linear regression was performed on the abundance of lymphoid cell subsets, with age, sex, and group (control, hospitalized, and outpatient) as independent variables. Across all three groups of adult blood donors, CD4+ T cells, CD8+

395 T cells, and ILCs decreased with age, while CD16$^+$ NK cells increased with age, and both

396 CD4$^+$ T cells and ILCs were less abundant in males (Table 2 and Fig. 3A).

397

398

Table 2: Change in Cell Abundance Due to Age, Sex, and COVID-19 Severity

Fold difference (log2) [±95%CI]

	CD4$^+$ T[a]	ILC[a]	CD8$^+$ T[a]	CD16$^+$ NK[a]
Age	-0.012***	-0.043***	-0.009*	0.021***
	[-0.018, -0.005]	[-0.053, -0.033]	[-0.016, -0.002]	[0.010, 0.032]
Male	-0.409***	-0.334*	-0.177	0.184
	[-0.618, -0.201]	[-0.659, -0.010]	[-0.406, 0.051]	[-0.169, 0.538]
Hospitalized	0.168	-0.835***	0.227	-1.205***
	[-0.084, 0.421]	[-1.228, -0.441]	[-0.050, 0.503]	[-1.633, -0.778]
Outpatient	0.332*	-0.088	-0.023	-0.522*
	[0.082, 0.581]	[-0.478, 0.302]	[-0.298, 0.253]	[-0.948, -0.095]
R^2	0.275	0.478	0.070	0.232

* $p < 0.05$, ** $p < 0.01$, *** $p < 0.001$
[a] per 10^6 lymphocytes

399

400

401

402

403

404

405

406   When effects of age and sex were held constant, adults hospitalized with COVID-

407   19 had 1.78-fold fewer ILCs (95%CI: 2.34–1.36; p = 4.55 x 10^{-5}) and 2.31-fold fewer

408    $CD16^+$ natural killer (NK) cells (95%CI: 3.1–1.71; p = 1.04 x 10^{-7}), as compared to controls

409   (Table 2 and Fig. 3B). Similar effects were also seen with ILC precursors (ILCP) (Figure

410   3–figure supplement 1). Neither $CD4^+$ T cells nor $CD8^+$ T cells were depleted further than

411   expected for age and sex (Table 2 and Fig. 3B). As compared with controls, SARS-CoV-

412   2-infected adults with less severe COVID-19 who were treated as outpatients had no

413   reduction in ILCs, but 1.44-fold fewer $CD16^+$ NK cells (95%CI: 1.93–1.07; p = 0.018), and

414   1.26-fold higher $CD4^+$ T cells (95%CI: 1.06–1.5; p = 9.59 x 10^{-3}) (Table 2 and Fig. 3B).

415   As these analyses were performed on lymphoid cell abundance normalized to total

416   lymphocyte number, it is possible that T cells were not lower in patients hospitalized with

417   COVID-19 because the amount of depletion was not in excess of the change in total

418   lymphocytes. However, the cell-type specific results remained unchanged even when the

419   analyses were repeated using the less stringent threshold of normalizing to total PBMC

420   number (Supplementary file 2e).

421   When data from an independent, previously published cohort (Kuri-Cervantes et

422   al., 2020) were analyzed to account for total lymphocyte abundance, age, and sex, people

423   hospitalized with acute respiratory distress syndrome due to COVID-19, had 1.7-fold

424   fewer ILCs (95%CI: 2.38–1.22; p = 0.002) than controls (Figure 3–figure supplement 2).

425   Also consistent with the main adult cohort studied here, ILC abundance was not

426   significantly reduced in the group of patients with less severe disease (Figure 3–figure

427   supplement 2).

428

429
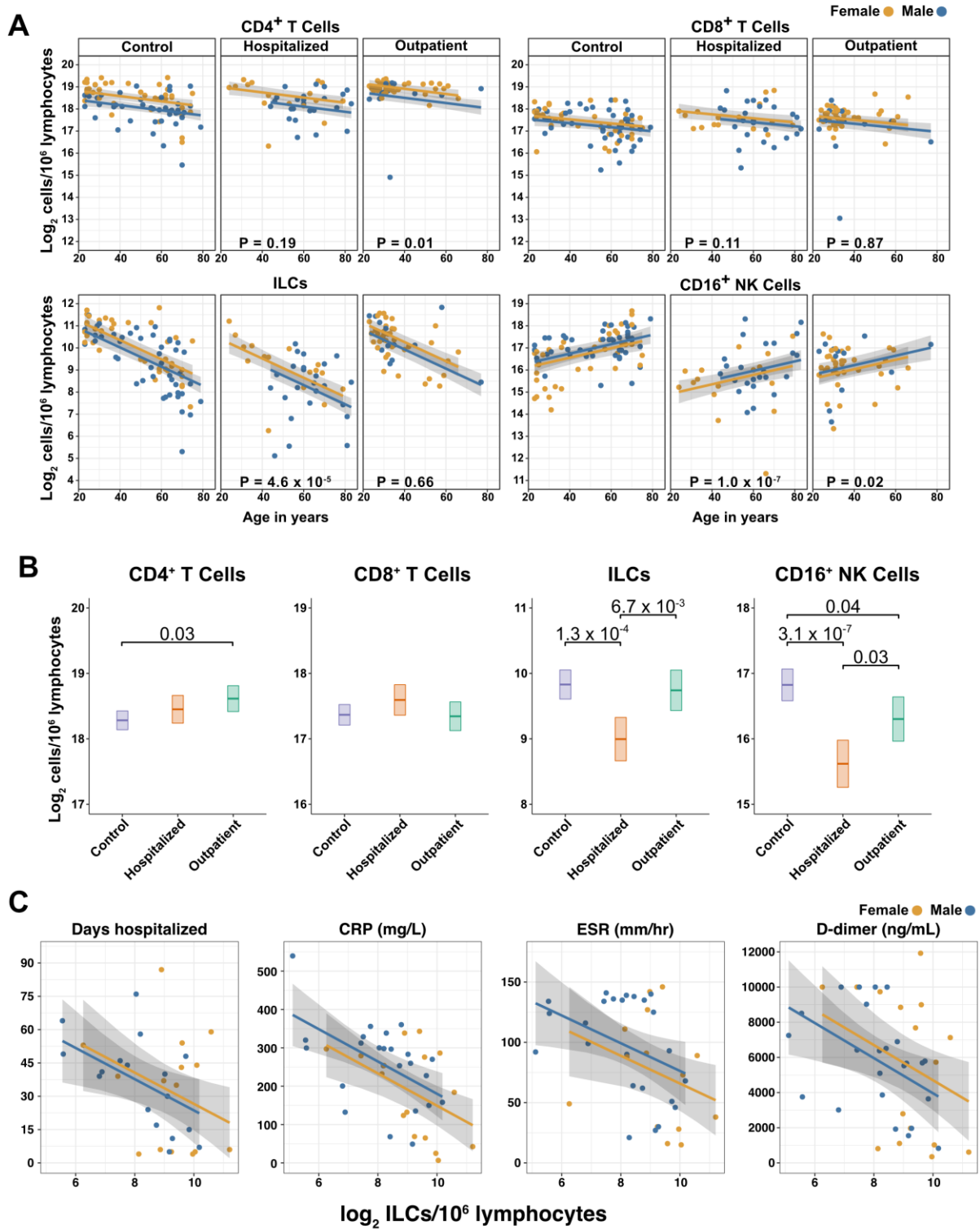
Fig. 3. Innate lymphoid cells are depleted in adults hospitalized with COVID-19 and ILC abundance correlates inversely with disease severity.

28

432 (**A**) Effect of age (X-axis) on log2 abundance per million total lymphocytes of the indicated

433 lymphoid cell populations (Y-axis), as determined by the regression analysis in Table 2.

434 Each dot represents an individual blood donor, with yellow for female and blue for male.

435 Shading represents the 95%CI. P-values are from the regression analysis for

436 comparisons to the control group.

437 (**B**) Log2 abundance per million lymphocytes of the indicated lymphoid cell populations,

438 shown as estimated marginal means with 95%CI, generated from the multiple linear

439 regressions in Table 2, and averaged across age and sex. P-values represent pairwise

440 comparisons on the estimated marginal means, adjusted for multiple comparisons with

441 the Tukey method. Adjusted P-values < 0.05 are shown.

442 (**C**) Association of the indicated clinical parameters with log2 abundance of ILCs per

443 million lymphoid cells. Regression lines are from simplified multiple regression models to

444 permit visualization on a two-dimensional plane. Shading represents the 95%CI. Results

445 of the full models accounting for effects of both age and sex, are reported in Table 4 and

446 the text.

447

448

449

450

451

452

Odds of hospitalization in adults infected with SARS-CoV-2 increases with

decreasing number of ILCs

Multiple logistic regression was used next to determine whether differences in abundance

of any lymphoid cell subset was associated with odds of hospitalization in people infected

with SARS-CoV-2. The adjusted odds ratio was calculated using lymphoid cell subset

abundance, age, sex, diagnosis of diabetes mellitus, and duration of symptoms at the

time of blood draw, each as independent variables. Abundance of ILCs, but not of CD16^{+}

NK cells, CD4^{+} T cells, or CD8^{+} T cells was associated with odds of hospitalization: the

odds ratio for hospitalization, adjusted for age, sex, diagnosis of diabetes mellitus, and

symptom duration, was 0.454 (95%CI: 0.213–0.808; p = 0.018), an increase of 54.6% for

each 2-fold decrease in ILC abundance (Table 3).

Table 3: Odds of Hospitalization[a]

Cell count[b]	Odds Ratio[c]	95% Confidence Interval	P-Value
CD4^{+} T	0.576	0.211–1.28	0.198
ILC	0.454	0.213–0.808	0.018
CD8^{+} T	1.2	0.584–3.06	0.652
CD16^{+} NK	0.841	0.538–1.27	0.412

[a]Adjusted for age, sex, diagnosis of diabetes mellitus, and symptom duration
at time of sample collection
[b]per 10[6] lymphocytes
[c]per 2-fold increase in cell population abundance

Duration of hospital stay in adults with COVID-19 increases with decreasing ILC abundance

The relationship between lymphoid cell abundance and duration of hospitalization was assessed to determine whether the association between ILC abundance and COVID-19 severity extended to clinical outcomes within the hospitalized adults. This relationship was assessed with multiple linear regression, including age, sex, and cell abundance as independent variables. Holding age and sex constant, abundance of ILCs, but not of CD16^{+} NK cells, CD4^{+} T cells, or CD8^{+} T cells, was associated with length of time in the hospital: each two-fold decrease in ILC abundance was associated with a 9.38 day increase in duration of hospital stay (95% CI: 15.76–3.01; p = 0.0054) (Fig. 3C and Table 4).

Table 4: Association of cell type abundance with time in hospital and laboratory values[a]

Cell count[b]	Days hospitalized	CRP (mg/L)[c]	ESR (mm/h)[c]	D-dimer (ng/mL)[c]
CD4^{+} T	-10.843	-3.335	-2.674	-1868.847*
	[-22.511, 0.825]	[-56.162, 49.492]	[-23.840, 18.492]	[-3375.630, -362.063]
ILC	-9.381**	-46.288***	-11.035*	-1098.515*
	[-15.755, -3.008]	[-71.337, -21.238]	[-21.936, -0.134]	[-1932.842, -264.188]
CD8^{+} T	3.366	32.247	15.317	486.192
	[-8.992, 15.724]	[-16.509, 81.003]	[-4.127, 34.761]	[-1049.836, 2022.221]
CD16^{+} NK	-4.775	-14.619	-5.159	-404.873
	[-11.251, 1.701]	[-44.011, 14.774]	[-16.809, 6.491]	[-1316.261, 506.516]

* $p < 0.05$, ** $p < 0.01$, *** $p < 0.001$
[a]coefficients are for each two-fold increase in cell population abundance, adjusted for age and sex [±95%CI]
[b]per 10^6 lymphoid cells
[c]Maximum lab value recorded during course of hospitalization

491

ILC abundance correlates inversely with markers of inflammation in adults hospitalized with COVID-19

To further characterize the extent to which lymphoid cell abundance predicted COVID-19 severity, multiple regression with age, sex, and cell abundance, as independent variables, was performed on peak blood levels of inflammation markers indicative of COVID-19 severity: C-reactive protein (CRP) and erythrocyte sedimentation rate (ESR), and the fibrin degradation product D-dimer (Gallo Marin et al., 2020; Gupta et al., 2021; Luo et al., 2020; Zhang et al., 2020; Zhou et al., 2020). Holding age and sex constant, each two-fold decrease in ILC, but not in CD16^{+} NK cell, CD4^{+} T cell, or CD8^{+} T cell abundance,

501 was associated with a 46.29 mg/L increase in blood CRP (95% CI: 71.34–21.24; p = 6.25

502 x 10^{-4}) and 11.04 mm/h increase in ESR (95% CI: 21.94–0.13; p = 0.047) (Fig. 3C and

503 Table 4). Abundance of both ILCs and CD4$^+$ T cells was associated with blood levels of

504 D-dimer, with each two-fold decrease in cell abundance associated with an increase in

505 D-dimer by 1098.52 ng/mL (95% CI: 1932.84–264.19; p = 0.011) and 1868.85 ng/mL

506 (95% CI: 3375.63–362.06; p = 0.016), respectively (Table 4).

507 **ILCs are depleted in children and young adults with COVID-19 or MIS-C**

508 Given the decline in ILC abundance with age (Fig.s 2A and 3A, and Table 2), and the

509 inverse relationship between ILC abundance and disease severity in adults (Fig. 3C,

510 Table 3, and Table 4), it was hypothesized that children as a group have less severe

511 COVID-19 because ILC abundance is higher at younger ages, and that pediatric cases

512 with symptomatic SARS-CoV-2 infection, or with MIS-C, are accompanied by significantly

513 lower numbers of ILCs. To test these hypotheses, the abundance of lymphoid cell subsets

514 in pediatric COVID-19 or MIS-C was compared with that from pediatric controls, using

515 multiple linear regression with age, sex, and group as independent variables. Consistent

516 with the findings in adults, blood ILCs in the pediatric cohort decreased with age (Table 5

517 and Fig. 4A), demonstrating that the decrease in ILC abundance across the lifespan is

518 already evident within the first two decades of life. In contrast, significant change over this

519 age range was not detected in the abundance of CD4$^+$ T cells, CD8$^+$ T cells, or CD16$^+$

520 NK cells (Table 5 and Fig 4A).

521   Among pediatric patients with COVID-19, no difference in abundance of the

522 lymphoid cell subsets was associated with hospitalization (Supplementary file 2f), so all

523 pediatric patients treated for COVID-19 were analyzed as a single group. After accounting

524   for effects of age and sex, pediatric patients with COVID-19 had 1.69-fold fewer ILCs

525   (95%CI: 2.73–1.04; p = 0.034) than controls (Fig 4A and Table 5). Neither CD4$^+$ T cells,

526   CD8$^+$ T cells, nor CD16$^+$ NK cells were depleted in pediatric COVID-19 patients (Fig 4A

527   and Table 5).

528   As with pediatric COVID-19, ILCs were also lower in MIS-C, with 2.14-fold fewer

529   ILCs (95%CI: 3.69–1.24; p = 0.007) than controls (Fig. 4A and Table 5). However, unlike

530   pediatric COVID-19, individuals with MIS-C had reduced numbers of T cells as compared

531   with pediatric controls, with 1.6-fold fewer CD4$^+$ T cells (95%CI: 2.04–1.26; p = 3.28x10$^-$

532   ^{4}) and 1.42-fold fewer CD8$^+$ T cells (95%CI: 1.87–1.07; p = 0.016) (Fig. 4A and Table 5).

533   Depletion of T cells, then, distinguished MIS-C from both pediatric and adult COVID-19.

534   Additionally, consistent with the finding in adults hospitalized with COVID-19 (Fig. 3C and

535   Table 4), after accounting for effect of group, each two-fold decrease in ILC abundance

536   in pediatric patients hospitalized with COVID-19 or MIS-C was associated with a 40.5

537   mg/L increase in blood CRP (95% CI: 77.87–3.13; p = 0.035) (Fig. 4C), and no such

538   association was detected with CD4$^+$ T cells, CD8$^+$ T cells, or CD16+ NK cells.

539

540

541

542

543

544

545

546

Table 5: Change in Pediatric Cohort Cell Abundance Due to Age, Sex, and Group

Fold difference (log2) [±95%CI]

	CD4^{+} T[a]	ILC[a]	CD8^{+} T[a]	CD16^{+} NK[a]
Age	-0.004	-0.083**	0.012	0.004
	[-0.027, 0.019]	[-0.135, -0.032]	[-0.014, 0.039]	[-0.060, 0.068]
Male	-0.219	-0.027	0.060	-0.343
	[-0.492, 0.054]	[-0.640, 0.586]	[-0.249, 0.370]	[-1.098, 0.413]
COVID	0.018	-0.754*	-0.088	0.416
	[-0.290, 0.327]	[-1.447, -0.061]	[-0.432, 0.257]	[-0.424, 1.257]
MIS-C	-0.678***	-1.098**	-0.503*	-0.498
	[-1.028, -0.328]	[-1.884, -0.313]	[-0.904, -0.101]	[-1.479, 0.483]
R^2	0.359	0.342	0.169	0.106

* $p < 0.05$, ** $p < 0.01$, *** $p < 0.001$
[a]per 10^6 lymphocytes

547

548

549   The above analysis of lymphoid cell subsets in pediatric COVID-19 and MIS-C was

550   performed in comparison to pediatric controls alone. Results were essentially unchanged

551   when multiple linear regression was repeated with combined pediatric and adult control

552   groups (Fig. 4B, Figure 4–figure supplement 1, and Supplementary file 2g).

553   **Pediatric MIS-C is distinguished from COVID-19 by recovery of ILCs during follow-**

554   **up**

555   The availability of follow-up samples in this pediatric cohort provided the opportunity to

556   assess the abundance of lymphoid subsets after recovery from illness. To this end, a

557   linear mixed model was fit to determine the change in ILC abundance from acute illness

558   to follow-up in 10 individuals (5 COVID-19 and 5 MIS-C) for whom both acute and follow-

559   up samples were available. After accounting for effects of age, sex, and group, individuals

560   recovering from MIS-C had a 2.39-fold increase in ILC abundance (95%CI: 1.49–3.81; p

561   = $6.6x10^{-3}$) but there was no significant change in ILC abundance for individuals

562   recovering from COVID-19 (Fig. 4D). Both CD4$^+$ and CD8$^+$ T cells, which were depleted

563   in MIS-C but not in COVID-19, also increased during recovery from MIS-C and remained

564   unchanged during recovery from COVID-19 (Figure 4–figure supplement 2).

565   The relationship between time to follow-up and lymphoid cell abundance was then

566   examined for all available follow-up samples whether or not a paired sample from the

567   acute illness was available (COVID-19, N=14; MIS-C, N=7). This analysis found no

568   relationship between time to follow-up and abundance of any lymphoid subset, and that

569   individuals recovering from MIS-C had 2.28-fold more ILCs (95%CI: 1.11–4.69; p =

570   0.0265) than individuals recovering from COVID-19 (Fig. 4E). Of note, ILC abundance

571   rebounded by 2 months of follow-up for the MIS-C patients, whereas ILC abundance still

572   had not rebounded after 9 months of follow-up for the COVID-19 patients. There was no

573   difference between the follow-up groups in CD4$^+$ T cells, CD8$^+$ T cells, or CD16$^+$ NK cells.

574   Interestingly, prior to being hospitalized with MIS-C, only one of these patients had

575   COVID-19 symptoms and, despite low ILC abundance in the COVID-19 follow-up cohort,

576   only 28.6% of this group had been ill enough to require hospitalization (Supplementary

577   file 2b).

578   Differences between COVID-19 and MIS-C in regards to T cell depletion and ILC

579   recovery during follow-up indicate that the underlying processes causing lower ILC

580   abundance in these two SARS-CoV-2-associated diseases are different.

581

582

Fig. 4. ILCs are depleted in children with COVID-19 or MIS-C
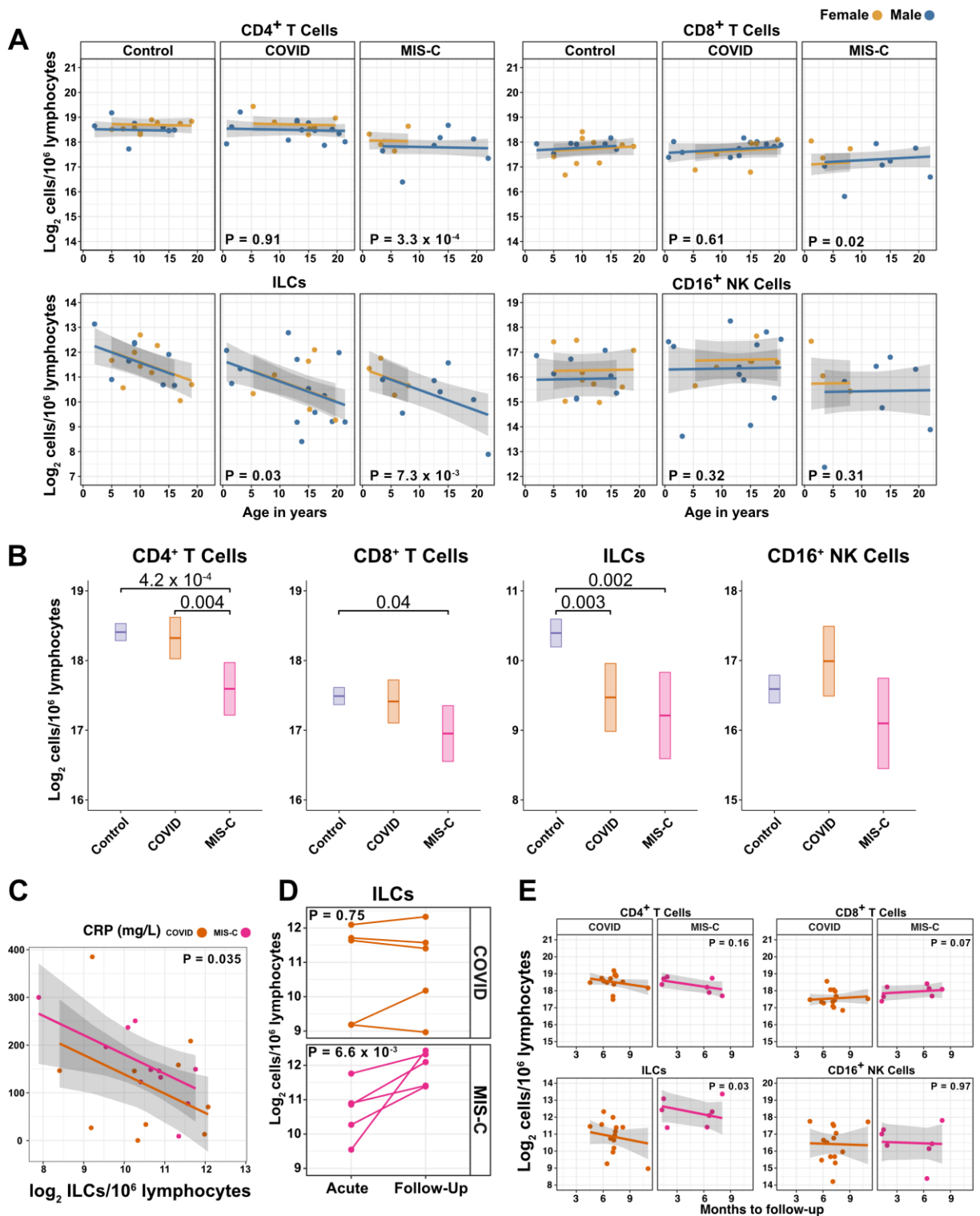
584   (**A**) Effect of age (X-axis) on log2 abundance per million lymphocytes of the indicated

585   lymphoid cell populations (Y-axis), as determined by the regression analysis in Table 5.

586   Each dot represents an individual blood donor, with yellow for female and blue for male.

587   Shading represents the 95%CI. P-values are from the regression analysis for

588   comparisons to the control group.

589   (**B**) Log2 abundance per million lymphocytes of the indicated lymphoid cell populations,

590   shown as estimated marginal means with 95%CI, generated from the multiple linear

591   regressions in file 2g that included the combined pediatric and adult control data, and

592   averaged across age and sex. P-values represent pairwise comparisons on the estimated

593   marginal means, adjusted for multiple comparisons with the Tukey method. Adjusted P-

594   values < 0.05 are shown.

595   (**C**) Association of CRP with log2 abundance of ILCs per million lymphocytes. Shading

596   represents the 95%CI. Each dot represents a single blood donor, orange for COVID-19,

597   magenta for MIS-C. P-value is for the effect of ILC abundance on CRP as determined by

598   linear regression.

599   (**D**) Log2 ILC abundance per million lymphocytes in longitudinal pairs of samples

600   collected during acute presentation and during follow-up, from individual children with

601   COVID-19 or MIS-C. Each pair of dots connected by a line represents an individual blood

602   donor. P-values are for change in ILC abundance at follow-up, as determined with a linear

603   mixed model, adjusting for age, sex, and group, and with patient as a random effect.

604   (**E**) Effect of time to follow-up (X-axis) on log2 abundance per million lymphocytes of the

605   indicated lymphoid cell populations (Y-axis). P-values are for the difference between the

606   COVID-19 and MIS-C follow-up groups, independent of time to follow-up as determined

607   by linear regression. Shading represents the 95%CI.

608

609   **Blood ILCs resemble homeostatic ILCs isolated from lung**

610   In response to the above results with blood ILCs, attempts were made to profile ILCs from

611   the lungs of people with fatal COVID-19, but isolation of ILCs from available samples was

612   unsuccessful. Given that ILCs circulate from tissues to the bloodstream via the thoracic

613   duct (Buggert et al., 2020), blood ILC levels might reflect tissue-resident cells and serve

614   as a surrogate for lung ILCs. While ILCs might be decreased in the blood as a result of

615   sequestration within the COVID-19-damaged lung (Ardain et al., 2019), reduced numbers

616   of ILCs within the intestinal lamina propria of people living with HIV-1 is paralleled by

617   reduction in blood ILCs (Wang et al., 2020).

618   Given the inability to assess lung samples from people with COVID-19, RNA

619   sequencing (RNA-Seq) was performed on blood ILCs from nine healthy controls and

620   these data were compared to previously published RNA-Seq profiles of ILCs sorted from

621   lung, spleen, and intestine (Ardain et al., 2019; Yudanin et al., 2019). Unbiased principal

622   component analysis demonstrated overlap of blood ILCs with ILCs from the lung, with

623   clear separation from ILCs of jejunum or spleen origin (Fig. 5A).

624   Based on expression of characteristic transcription factors and specific inducible

625   cytokines, ILCs are classified into ILC1, ILC2, and ILC3 subsets that are analogous to

626   T_H1, T_H2, and T_H17 cells respectively (Artis and Spits, 2015; Cherrier et al., 2018; Vivier

627   et al., 2018; Yudanin et al., 2019). 355 genes were consistently differentially expressed

628   (fold-change > 1.5, padj < 0.01) when either blood or lung ILCs were compared to ILCs

629   from the other tissues (Fig. 5B,C). Gene ontology analysis demonstrated enrichment for

630   terms associated with type 2 immunity (Supplementary file 2h). Genes significantly higher

631   in both blood and lung ILCs included the ILC2-defining genes GATA3 and PTGDR2

632   (CRTH2), as well as other genes important for ILC development such as TCF7 (Yang et

633   al., 2013) (Fig. 5B,C).

634   TCF7- and CRTH2-encoded proteins were detected in blood ILCs by flow

635   cytometry, confirming the RNA signature of ILC2s (Fig. 6A). To assess the function of

636   blood ILCs, PBMCs were stimulated with PMA and ionomycin, and assayed by flow

637   cytometry for production of IL-13 after intracellular cytokine staining and gating on ILCs.

638   IL-13 was detected in the stimulated ILC population (Fig. 6B), demonstrating that the

639   majority of blood ILCs function as ILC2s. Additionally, the blood ILCs produced

640   amphiregulin (Fig. 6B), a protein implicated in the promotion of disease tolerance by ILCs

641   in animal models (Branzk et al., 2018; Diefenbach et al., 2020; Jamieson et al., 2013;

642   McCarville and Ayres, 2018; Monticelli et al., 2015, 2011).

643
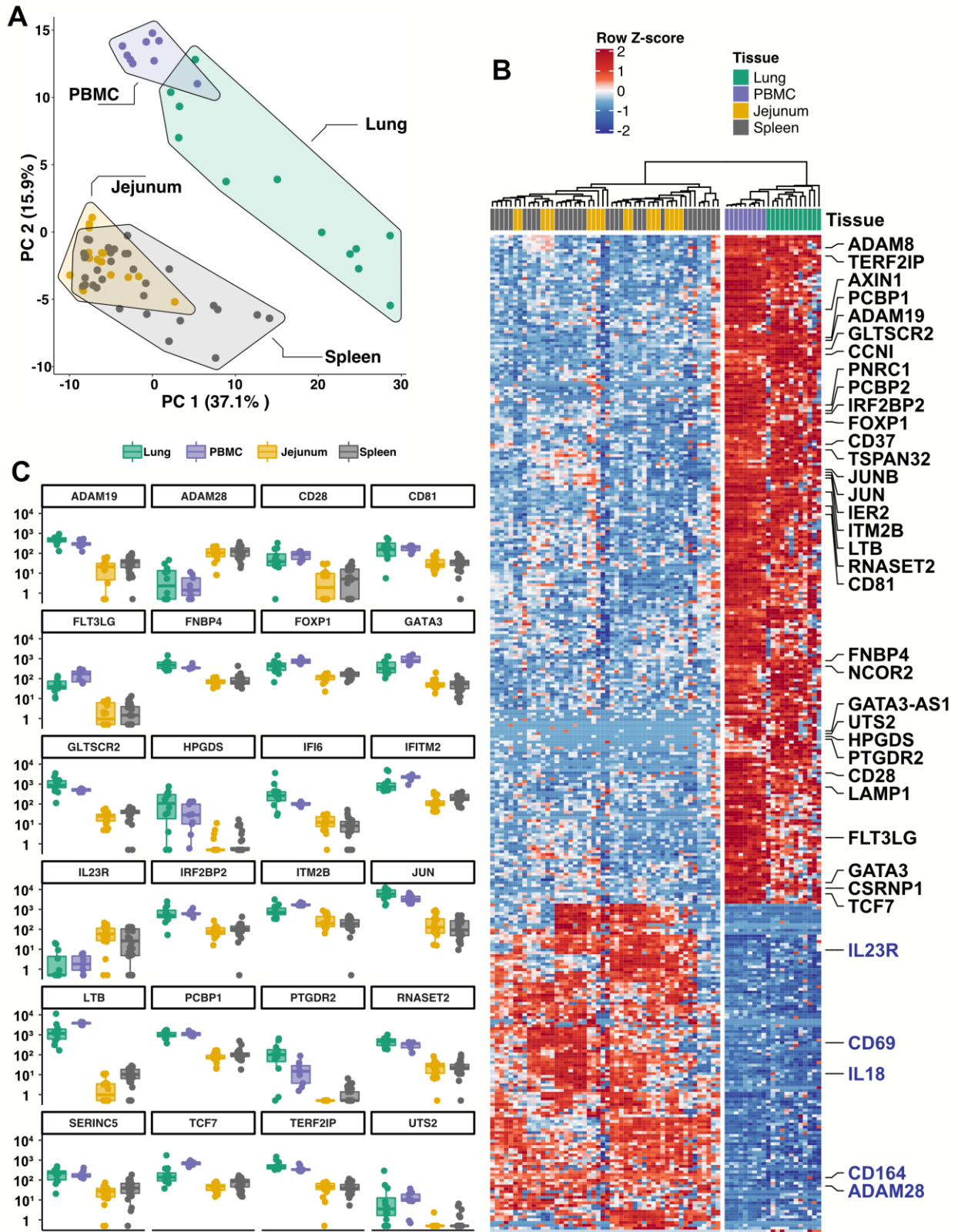
Fig. 5. Blood ILCs are transcriptionally similar to lung ILCs

645   RNA-seq of ILCs sorted from blood of 9 SARS-CoV-2-uninfected controls in comparison

646   to RNA-seq data of ILCs sorted from jejunum, lung, and spleen.

647   (**A**) PCA plot of first two principal components calculated from the top 250 most variable

648   genes across all samples. Each dot represents an individual sample with blue for ILCs

649   sorted from blood, green for lung, yellow for jejunum, and grey for spleen.

650   (**B**) Heatmap of 355 genes differentially expressed (fold-change > 1.5, padj < 0.01 as

651   determined with DESeq2) between either blood or lung ILCs and ILCs from the other

652   tissues.

653   (**C**) Select genes from (B) plotted as deseq2 normalized counts. Each dot represents an

654   individual sample with blue for ILCs sorted from blood, green for lung, yellow for jejunum,

655   and grey for spleen. Boxplots represent the distribution of the data with the center line

656   drawn through the median with the upper and lower bounds of the box at the 75th and

657   25th percentiles respectively. The upper and lower whiskers extend to the largest or

658   smallest values within 1.5 x the interquartile range (IQR).

659

660

661

662

663

664

665 **Effect of sex and COVID-19 on fraction of blood ILCs that produce amphiregulin**

666 Given the role that AREG-producing ILCs play in maintaining disease tolerance in animal

667 models (Branzk et al., 2018; Diefenbach et al., 2020; McCarville and Ayres, 2018;

668 Monticelli et al., 2015, 2011), sex differences in the functional capability of these ILCs

669 could contribute to the greater risk for severe COVID-19 in males (O'Driscoll et al., 2020).

670 To address this hypothesis, ILCs isolated from the peripheral blood of controls were

671 stimulated with PMA and ionomycin, and assayed by flow cytometry for AREG production.

672 Consistent with the apparently lower disease tolerance in males, males had a lower

673 median fraction of AREG$^+$ ILCs than did females ($p = 0.018$) (Fig. 6C). This difference

674 was also reflected in a significantly lower AREG Mean Fluorescent Intensity (MFI) in

675 males, and neither fraction of AREG$^+$ ILCs nor AREG MFI was affected by age (Figure

676 6–figure supplement 1). Multiple linear regression was performed, with age, sex, and

677 group as independent variables, to determine whether hospitalization with COVID-19 was

678 associated with differences in the percentage of AREG$^+$ ILCs. This analysis showed that,

679 after accounting for effects of age and sex, patients hospitalized with COVID-19 had a

680 1.91-fold lower percentage of AREG$^+$ ILCs (95%CI: 1.19–3.06; $p = 8.06 \times 10^{-3}$) than
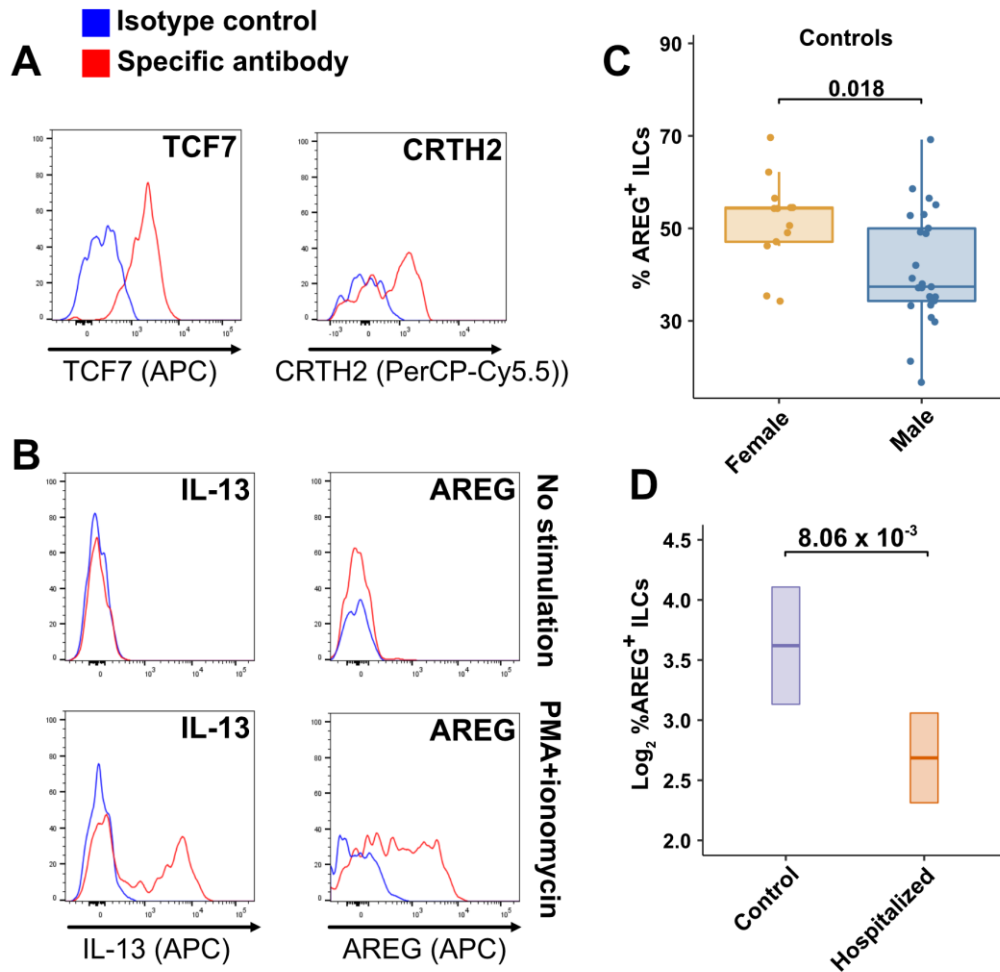
681 controls (Fig. 6D).

682
683
684

685

686

687

688

689

Fig. 6. Peripheral blood ILCs exhibit homeostatic ILC2 functions

(**A-B**) Flow cytometry for the indicated proteins. Cells in (**A**) were assayed at steady-state and cells in (**B**) were assayed either at steady-state or after stimulation with PMA and ionomycin, as indicated. Detection of surface proteins was performed on ILCs gated as Lin⁻CD56⁻CD127⁺ and detection of intracellular proteins was performed on ILCs gated as Lin⁻TBX21⁻CD127⁺.

(**C**) Percent of AREG⁺ ILCs in blood of control blood donors after stimulation with PMA and ionomycin and gated as Lin⁻TBX21⁻CD127⁺. Each dot represents an individual blood donor (N Female = 13, N Male = 25). Boxplots represent the distribution of the data with the center line drawn through the median with the upper and lower bounds of the box at

700 the 75th and 25th percentiles respectively. The upper and lower whiskers extend to the

701 largest or smallest values within 1.5 x the interquartile range (IQR). P-value is from a two-

702 sided, Wilcoxon rank-sum test.

703 (**D**) Log 2 percent AREG$^+$ ILCs in blood of control and hospitalized blood donors after

704 stimulation with PMA and ionomycin and gated as Lin$^-$TBX21$^-$. Data shown as estimated

705 marginal means with 95%CI, generated from the multiple linear regression reported in the

706 text and averaged across age and sex. P-value is from the regression analysis.

707

708

709

710
711

712

713

714
715
716
717
718
719
720
721
722
723

DISCUSSION

The outcome of SARS-CoV-2 infection ranges from entirely asymptomatic to lethal COVID-19 (Cevik et al., 2021; He et al., 2021; Jones et al., 2021; Lee et al., 2020; Lennon et al., 2020; Ra et al., 2021; Richardson et al., 2020; Yang et al., 2021). Yet, viral load does not reliably discriminate asymptomatic from symptomatic or hospitalized populations (Cevik et al., 2021; Jones et al., 2021; Lee et al., 2020; Lennon et al., 2020; Ra et al., 2021; Yang et al., 2021). In contrast, demographic factors, including increasing age and male sex, predict worse outcome of SARS-CoV-2 infection (Alkhouli et al., 2020; Bunders and Altfeld, 2020; Gupta et al., 2021; Laxminarayan et al., 2020; Mauvais-Jarvis, 2020; O'Driscoll et al., 2020; Peckham et al., 2020; Richardson et al., 2020; Scully et al., 2020). These demographic risk factors could be due to sexual dimorphism and changes with aging in composition and function of the human immune system (Darboe et al., 2020; Klein and Flanagan, 2016; Márquez et al., 2020; Patin et al., 2018; Solana et al., 2012). Therefore it is necessary to account for effects of age and sex to determine if there are additional, independent, effects of SARS-CoV-2-associated disease.

This study collected and analyzed 245 blood samples from 177 adult and 58 pediatric patients and controls, spanning the ages of 0.7 to 83 years, with approximately equal numbers of males and females. It was therefore possible to characterize the independent effects of age, sex, COVID-19, and MIS-C on blood lymphoid cell populations. After accounting for effects of age and sex, ILCs, but not CD4$^+$ or CD8$^+$ T cells, were lower in individuals hospitalized with COVID-19 when compared with controls (Table 2 and Fig. 3A,B). Lower numbers of ILCs were also observed in children with COVID-19 (Table 5 and Fig. 4A,B), as well as in an independent cohort of adult patients

47

747   (Figure 3–figure supplement 2). Among adults infected with SARS-CoV-2, lower

748   abundance of ILCs, but not of the other lymphoid cell subsets, was associated with

749   increased odds of hospitalization, longer duration of hospitalization, and higher blood

750   level of factors associated with systemic inflammation, including CRP (Tables 3 and 4,

751   and Fig. 3C). This inverse relationship between ILC abundance and CRP was also

752   evident in children with COVID-19 or MIS-C (Fig. 4C).

753   The identification of reduced ILC numbers as uniquely related to COVID-19

754   severity is important as these cells mediate disease tolerance in animal models (Artis and

755   Spits, 2015; Branzk et al., 2018; Califano et al., 2018; Diefenbach et al., 2020; McCarville

756   and Ayres, 2018; Monticelli et al., 2015, 2011). The results here therefore indicate that

757   loss of ILCs from blood correlates with loss of ILC-associated homeostatic functions,

758   thereby allowing more severe COVID-19. Although this study examined circulating blood

759   lymphoid cells, and does not provide direct information about processes occurring within

760   tissues, transcriptional and functional characterization of blood ILCs demonstrated that

761   these cells are similar to ILCs isolated from lung tissue (Fig. 5). Human ILCs circulate in

762   lymphatic fluid draining from the tissues to the blood via the thoracic duct (Buggert et al.,

763   2020), raising the possibility that some ILCs in the blood originate from, or traffic to, lung

764   tissue. Further characterization of these blood ILCs showed that they are functional ILC2s

765   capable of producing the protein AREG (Fig. 6A,B). Given the tissue homeostatic role

766   AREG plays in animal models of disease tolerance (Branzk et al., 2018; Diefenbach et

767   al., 2020; Jamieson et al., 2013; McCarville and Ayres, 2018; Monticelli et al., 2015,

768   2011), the discovery here that males have a smaller fraction than females of blood ILCs

769   capable of producing AREG (Fig. 6C) could explain why males are at greater risk of death

770 from SARS-CoV-2 infection (O'Driscoll et al., 2020). This sexual dimorphism in ILC

771 function would be amplified further by the lower overall abundance of ILCs in males (Fig.

772 2B and Table 3).

773   Although the inverse relationship between the number of blood ILCs and severity

774 of COVID-19 suggests that loss of ILC homeostatic function results in breakdown of

775 disease tolerance (Arpaia et al., 2015; Artis and Spits, 2015; Branzk et al., 2018;

776 Diefenbach et al., 2020; McCarville and Ayres, 2018; Monticelli et al., 2015, 2011), this

777 observational study cannot determine whether ILC depletion preceded SARS-CoV-2

778 infection or whether ILC numbers are depleted as a consequence of SARS-CoV-2

779 infection. However, several observations support the hypothesis that individuals with

780 lower ILC numbers at the time of SARS-CoV-2 infection are at greater risk of developing

781 severe disease. ILC numbers in uninfected controls decrease exponentially with age; this

782 decrease is much larger than that seen with other lymphoid cell types (Fig. 2A), and much

783 more closely mirrors the exponential increase in COVID-19 mortality with age(O'Driscoll

784 et al., 2020) (Fig. 2C). In addition, the greater risk of COVID-19 mortality in males

785 (O'Driscoll et al., 2020) correlates with lower abundance of blood ILCs (Fig. 2B and Table

786 3) and smaller fraction of ILCs capable of producing AREG (Fig. 6C). Finally, patients

787 hospitalized with COVID-19 have a smaller fraction of AREG[+] ILCs than controls (Fig.

788 6D) and conditions independently associated with lower ILC abundance, such as HIV-1

789 infection (Kløverpris et al., 2016; Wang et al., 2020) and obesity (Brestoff et al., 2015;

790 Yudanin et al., 2019), increase the risk for worse outcomes from SARS-CoV-2 infection

791 (Biccard et al., 2021; Kompaniyets, 2021; Tesoriero et al., 2021).

792   In contrast to individuals with COVID-19, children with MIS-C had lower numbers

793 of T cells as well as ILCs (Table 5 and Fig. 4A,B), and longitudinal follow-up samples for

794 pediatric COVID-19 and MIS-C patients showed persistence of low ILC numbers after

795 COVID-19, but normalization of all depleted cell types after recovery from MIS-C (Fig.

796 4D,E and Figure 4–figure supplement 2). These differences imply that the reversible

797 lymphopenia in MIS-C is due to different underlying processes than the more specific and

798 persistent lower ILC abundance seen in individuals with COVID-19. This difference is

799 made more interesting by the fact that none of the children with MIS-C had required

800 hospitalization for COVID-19 and only one experienced any COVID-19 symptoms. The

801 other children with MIS-C were therefore unaware that they had been infected. It is

802 possible that children with pre-existing lower ILC numbers are at risk of developing

803 COVID-19 if infected with SARS-CoV-2, while other factors such as prolonged exposure

804 to SARS-CoV-2 antigens in the gastrointestinal tract (Yonker et al., 2021), or rare inborn

805 errors of immunity (Sancho-Shimizu et al., 2021), promote inflammatory processes in

806 MIS-C that drive nonspecific lymphoid cell depletion, which ultimately normalizes after

807 recovery.

808   Although ILC depletion and recovery has been reported in rheumatoid arthritis

809 (Rauber et al., 2017), inflammation-driven ILC-depletion is not necessarily reversible, as

810 ILCs appear permanently depleted after HIV-1 infection, possibly by the high levels of

811 common γ-chain cytokines that are present during acute infection (Wang et al., 2020).

812 Better understanding of the processes that drive down ILC abundance in populations

813 susceptible to COVID-19 could potentially allow for development of interventions that

814 increase ILC abundance and restore homeostatic disease tolerance mechanisms.

815   In conclusion, considering the established functions of ILCs (Artis and Spits, 2015;

816   Branzk et al., 2018; Klose and Artis, 2016; Monticelli et al., 2015, 2011), and the host

817   homeostatic responses necessary to survive pathogenic infection (López-Otín and

818   Kroemer, 2021; McCarville and Ayres, 2018; Medzhitov et al., 2012; Schneider and

819   Ayres, 2008), the findings reported here support the hypothesis that loss of disease

820   tolerance mechanisms attributable to ILCs increase the risk of morbidity and mortality

821   with SARS-CoV-2 infection. The findings of this observational study warrant

822   establishment of prospective cohorts to determine whether abundance of ILCs or of other

823   lymphoid cell subsets associated with disease tolerance (Arpaia et al., 2015; Artis and

824   Spits, 2015; Branzk et al., 2018; Diefenbach et al., 2020; McCarville and Ayres, 2018;

825   Monticelli et al., 2015, 2011), predict clinical outcome for infection with SARS-CoV-2 or

826   other lethal pathogens. Understanding the mechanisms that allow an individual to tolerate

827   high-level viral replication without experiencing symptoms, and how these mechanisms

828   can fail and thereby allow for progression to severe disease, will provide the foundation

829   for development of therapeutic interventions that maintain health and improve survival of

830   pathogenic viral infection (Ayres, 2020b).

831

832

833

834

835

836

837

838

839 **REFERENCES**

840 Alghamdi IG, Hussain II, Almalki SS, Alghamdi MS, Alghamdi MM, El-Sheemy MA. 2014. The

841   pattern of Middle East respiratory syndrome coronavirus in Saudi Arabia: a descriptive

842   epidemiological analysis of data from the Saudi Ministry of Health. *Int J Gen Med* **7**:417.

843 Alkhouli M, Nanjundappa A, Annie F, Bates MC, Bhatt DL. 2020. Sex Differences in Case

844   Fatality Rate of COVID-19: Insights From a Multinational Registry. *Mayo Clin Proc*

845   **95**:1613–1620.

846 Anegon I, Cuturi MC, Trinchieri G, Perussia B. 1988. Interaction of Fc receptor (CD16) ligands

847   induces transcription of interleukin 2 receptor (CD25) and lymphokine genes and

848   expression of their products in human natural killer cells. *J Exp Med* **167**:452–472.

849 Ardain A, Domingo-Gonzalez R, Das S, Kazer SW, Howard NC, Singh A, Ahmed M,

850   Nhamoyebonde S, Rangel-Moreno J, Ogongo P, Lu L, Ramsuran D, de la Luz Garcia-

851   Hernandez M, K. Ulland T, Darby M, Park E, Karim F, Melocchi L, Madansein R, Dullabh

852   KJ, Dunlap M, Marin-Agudelo N, Ebihara T, Ndung'u T, Kaushal D, Pym AS, Kolls JK,

853   Steyn A, Zúñiga J, Horsnell W, Yokoyama WM, Shalek AK, Kløverpris HN, Colonna M,

854   Leslie A, Khader SA. 2019. Group 3 innate lymphoid cells mediate early protective

855   immunity against tuberculosis. *Nature* **570**:528–532.

856 Arpaia N, Green JA, Moltedo B, Arvey A, Hemmers S, Yuan S, Treuting PM, Rudensky AY.

857   2015. A Distinct Function of Regulatory T Cells in Tissue Protection. *Cell* **162**:1078–

858   1089.

859 Artis D, Spits H. 2015. The biology of innate lymphoid cells. *Nature* **517**:293–301.

860 Ayres JS. 2020a. The Biology of Physiological Health. *Cell* **181**:250–269.

861 Ayres JS. 2020b. Surviving COVID-19: A disease tolerance perspective. *Sci Adv* **6**:eabc1518.

862 Bates D, Mächler M, Bolker B, Walker S. 2015. Fitting Linear Mixed-Effects Models Usinglme4.

863   *Journal of Statistical Software*. doi:10.18637/jss.v067.i01

864 Biccard BM, Gopalan PD, Miller M, Michell WL, Thomson D, Ademuyiwa A, Aniteye E, Calligaro

865   G, Chaibou MS, Dhufera HT, Elfagieh M, Elfiky M, Elhadi M, Fawzy M, Fredericks D,

866   Gebre M, Bayih AG, Hardy A, Joubert I, Kifle F, Kluyts H-L, Macleod K, Mekonnen Z,

867   Mer M, Morais A, Msosa V, Mulwafu W, Ndonga A, Ngumi Z, Omigbodun A, Owoo C,

868   Paruk F, Piercy JL, Scribante J, Seman Y, Taylor E, van Straaten D, Elfiky M, Fawzy M,

869   Awad A, Hussein H, Shaban M, Elbadawy M, Elmehrath AO, Cordie A, Elganainy M, El-

870   Shazly M, Essam M, Abdelwahab OA, Ali A, Hussein AM, Kamel EZ, Monib FA, Ahmed

871   I, Saad MM, Al-Quossi MA, Rafaat N, Galal I, Labib B, Omran DO, Fawzy M, Elfiky M,

872   Azzam Ahmed, Azab M, Tawheed A, Gamal M, El Kassas M, Azzam Aml, Ahmed N,

873   NasrEldin Y, Abdewahab O, Elganainy M, Elmandouh O, Dhufera HT, MeGebre M,

874   Bayih AG, Kifle F, Mekonnen Z, Seman Y, Addisie A, Eshete A, Kifle F, Desita K, Araya

875   H, Agidew Y, Andabo AD, Tesfaye E, Yesuf EA, Hailemariam G, Mohammed MS,

876   Gebremedhin Y, Taye Y, Mebrate TA, Gemechu TB, Bedane TT, Abera ET, Teshome A,

877   Ernest Aniteye EA, Christian Owoo CO, Doku A, Owoo C, Afriyie-Mensah JS, Lawson A,

878   Owoo C, DYaw Sottie DA, Addae E, Ernest Ofosu-Appiah EO-A, William Obeng WO,

879   Ndonga A, Ngumi Z, Ndonga A, Mugera A, Bitta C, Elfagieh M, Elhadi M, Huwaysh MA,

880   Yahya MMA, Mohammed AAK, Majeed AAM, Mohammed AEM, Majeed E, Abusalama

881   AA, Altayr E, Abubaker T, Alkaseek AM, Abdulhafith B, Alziyituni Z, Gamra MF, Anaiba

882   MM, Khel S, Abdelkabir M, Abdeewi S, Adam S, Alhadi A, Alsoufi A, Hassan M,

883   Msherghi A, Bouhuwaish AEM, Msosa V, Mulwafu W, Masoo F, Chikumbanje SS,

884   Mabedi D, Morais A, Carlos A, Morais A, Lorenzoni C, Mambo J, Isabel Chissaque I,

885   Mouzinho Saide M, Chaibou MS, Mamane M, Amadou F, Adesoji Ademuyiwa AA,

886   Akinyinka Omigbodun AO, Adeyeye A, Akinmade A, Momohsani Y, Bamigboye J,

887   Orshio D, Isamade ES, Embu H, Nuhu S, Ojiakor S, Nuhu A, Fowotade A, Sanusi A,

888   Osinaike B, Idowu O, Amali AO, Ibrahim S, Adamu AA, Kida I, Otokwala J, Essam M,

889   Alagbe-Briggs O, Ojum S, Fathima Paruk FP, Juan Scribante JS, Mdladla A, Mabotja T,

890   Naidoo R, Matos-Puig R, Ramkillawan A, Smith M, Arnold-Day C, Thomson D, Calligaro

891   G, Joubert I, Jagga J, Piercy J, Michell L, Devenish L, Miller M, Fernandes N, Gopalan

892   D, Pershad S, Grabowski N, Rammego M, Zwane S, Dhlamini ME, Neuhoff M, Fodo T,

893   Usenbo A, Mrara B, Kabambi F, Cloete E, De Caires L, Dickerson R, Louw C, Theron A,

894   Herselman R, Badenhorst J, Moletsane G, Loots H, Paruk F, Chausse J, Neuhoff M,

895   Sebastian M, Grabowski N, Rheeder P, van Hougenhouck-Tulleken W, Snyman C,

896   Adeleke D, Esterhuizen J, de Man L, Mosola M, van der Linde P, Swart R, Maasdorp S,

897   Martins T, Govender V. 2021. Patient care and clinical outcomes for patients with

898   COVID-19 infection admitted to African high-care or intensive care units (ACCCOS): a

899   multicentre, prospective, observational cohort study. *Lancet* **397**:1885–1894.

900   Bonnet B, Cosme J, Dupuis C, Coupez E, Adda M, Calvet L, Fabre L, Saint-Sardos P, Bereiziat

901   M, Vidal M, Laurichesse H, Souweine B, Evrard B. 2021. Severe COVID-19 is

902   characterized by the co-occurrence of moderate cytokine inflammation and severe

903   monocyte dysregulation. *EBioMedicine* **73**:103622.

904   Branzk N, Gronke K, Diefenbach A. 2018. Innate lymphoid cells, mediators of tissue

905   homeostasis, adaptation and disease tolerance. *Immunol Rev* **286**:86–101.

906   Brestoff JR, Kim BS, Saenz SA, Stine RR, Monticelli LA, Sonnenberg GF, Thome JJ, Farber

907   DL, Lutfy K, Seale P, Artis D. 2015. Group 2 innate lymphoid cells promote beiging of

908   white adipose tissue and limit obesity. *Nature* **519**:242–246.

909   Buggert M, Vella LA, Nguyen S, Wu VH, Chen Z, Sekine T, Perez-Potti A, Maldini CR, Manne

910   S, Darko S, Ransier A, Kuri-Cervantes L, Japp AS, Brody IB, Ivarsson MA, Gorin J-B,

911   Rivera-Ballesteros O, Hertwig L, Antel JP, Johnson ME, Okoye A, Picker L, Vahedi G,

912   Sparrelid E, Llewellyn-Lacey S, Gostick E, Sandberg JK, Björkström N, Bar-Or A, Dori Y,

913   Naji A, Canaday DH, Laufer TM, Wells AD, Price DA, Frank I, Douek DC, Wherry EJ,

914   Itkin MG, Betts MR. 2020. The Identity of Human Tissue-Emigrant CD8+ T Cells. *Cell*

915   **183**:1946-1961.e15.

916   Bunders MJ, Altfeld M. 2020. Implications of Sex Differences in Immunity for SARS-CoV-2

917   Pathogenesis and Design of Therapeutic Interventions. *Immunity* **53**:487–495.

918   Califano D, Furuya Y, Roberts S, Avram D, McKenzie ANJ, Metzger DW. 2018. IFN-γ increases

919   susceptibility to influenza A infection through suppression of group II innate lymphoid

920   cells. *Mucosal Immunol* **11**:209–219.

921   CDC Case Surveillance Task Force. 2020. COVID-19 Case Surveillance Public Use Data.

922   Cevik M, Tate M, Lloyd O, Maraolo AE, Schafers J, Ho A. 2021. SARS-CoV-2, SARS-CoV, and

923   MERS-CoV viral load dynamics, duration of viral shedding, and infectiousness: a

924   systematic review and meta-analysis. *The Lancet Microbe* **2**:e13–e22.

925   Channappanavar R, Fett C, Mack M, Ten Eyck PP, Meyerholz DK, Perlman S. 2017. Sex-

926   Based Differences in Susceptibility to Severe Acute Respiratory Syndrome Coronavirus

927   Infection. *J Immunol* **198**:4046–4053.

928   Charles Bailey L, Razzaghi H, Burrows EK, Timothy Bunnell H, Camacho PEF, Christakis DA,

929   Eckrich D, Kitzmiller M, Lin SM, Magnusen BC, Newland J, Pajor NM, Ranade D, Rao S,

930   Sofela O, Zahner J, Bruno C, Forrest CB. 2020. Assessment of 135 794 Pediatric

931   Patients Tested for Severe Acute Respiratory Syndrome Coronavirus 2 Across the

932   United States. *JAMA Pediatr*. doi:10.1001/jamapediatrics.2020.5052

933   Chen G, Wu D, Guo W, Cao Y, Huang D, Wang H, Wang T, Zhang Xiaoyun, Chen H, Yu H,

934   Zhang Xiaoping, Zhang M, Wu S, Song J, Chen T, Han M, Li S, Luo X, Zhao J, Ning Q.

935   2020. Clinical and immunological features of severe and moderate coronavirus disease

936   2019. *J Clin Invest* **130**:2620–2629.

937   Chen J, Subbarao K. 2007. The Immunobiology of SARS. *Annu Rev Immunol* **25**:443–472.

938   Cherrier DE, Serafini N, Di Santo JP. 2018. Innate Lymphoid Cell Development: A T Cell

939   Perspective. *Immunity* **48**:1091–1103.

940   Cheung EW, Zachariah P, Gorelik M, Boneparth A, Kernie SG, Orange JS, Milner JD. 2020.

941   Multisystem Inflammatory Syndrome Related to COVID-19 in Previously Healthy

942   Children and Adolescents in New York City. *JAMA* **324**:294–296.

943 Cumnock K, Gupta AS, Lissner M, Chevee V, Davis NM, Schneider DS. 2018. Host Energy

944   Source Is Important for Disease Tolerance to Malaria. *Curr Biol* **28**:1635-1642.e3.

945 Darboe A, Nielsen CM, Wolf A-S, Wildfire J, Danso E, Sonko B, Bottomley C, Moore SE, Riley

946   EM, Goodier MR. 2020. Age-Related Dynamics of Circulating Innate Lymphoid Cells in

947   an African Population. *Front Immunol* **11**:594107.

948 Diefenbach A, Gnafakis S, Shomrat O. 2020. Innate Lymphoid Cell-Epithelial Cell Modules

949   Sustain Intestinal Homeostasis. *Immunity* **52**:452–463.

950 Dobin A, Davis CA, Schlesinger F, Drenkow J, Zaleski C, Jha S, Batut P, Chaisson M, Gingeras

951   TR. 2013. STAR: ultrafast universal RNA-seq aligner. *Bioinformatics* **29**:15–21.

952 Donnelly CA, Ghani AC, Leung GM, Hedley AJ, Fraser C, Riley S, Abu-Raddad LJ, Ho L-M,

953   Thach T-Q, Chau P, Chan K-P, Lam T-H, Tse L-Y, Tsang T, Liu S-H, Kong JHB, Lau

954   EMC, Ferguson NM, Anderson RM. 2003. Epidemiological determinants of spread of

955   causal agent of severe acute respiratory syndrome in Hong Kong. *Lancet* **361**:1761–

956   1766.

957 D'Souza SS, Shen X, Fung ITH, Ye L, Kuentzel M, Chittur SV, Furuya Y, Siebel CW, Maillard

958   IP, Metzger DW, Yang Q. 2019. Compartmentalized effects of aging on group 2 innate

959   lymphoid cell development and function. *Aging Cell*. doi:10.1111/acel.13019

960 Feldstein LR, Rose EB, Horwitz SM, Collins JP, Newhams MM, Son MBF, Newburger JW,

961   Kleinman LC, Heidemann SM, Martin AA, Singh AR, Li S, Tarquinio KM, Jaggi P, Oster

962   ME, Zackai SP, Gillen J, Ratner AJ, Walsh RF, Fitzgerald JC, Keenaghan MA, Alharash

963   H, Doymaz S, Clouser KN, Giuliano JS Jr, Gupta A, Parker RM, Maddux AB, Havalad V,

964   Ramsingh S, Bukulmez H, Bradford TT, Smith LS, Tenforde MW, Carroll CL, Riggs BJ,

965   Gertz SJ, Daube A, Lansell A, Coronado Munoz A, Hobbs CV, Marohn KL, Halasa NB,

966   Patel MM, Randolph AG, Overcoming COVID-19 Investigators, CDC COVID-19

967   Response Team. 2020. Multisystem Inflammatory Syndrome in U.S. Children and

968   Adolescents. *N Engl J Med* **383**:334–346.

969   Feldstein LR, Tenforde MW, Friedman KG, Newhams M, Rose EB, Dapul H, Soma VL, Maddux

970   AB, Mourani PM, Bowens C, Maamari M, Hall MW, Riggs BJ, Giuliano JS Jr, Singh AR,

971   Li S, Kong M, Schuster JE, McLaughlin GE, Schwartz SP, Walker TC, Loftis LL, Hobbs

972   CV, Halasa NB, Doymaz S, Babbitt CJ, Hume JR, Gertz SJ, Irby K, Clouser KN,

973   Cvijanovich NZ, Bradford TT, Smith LS, Heidemann SM, Zackai SP, Wellnitz K, Nofziger

974   RA, Horwitz SM, Carroll RW, Rowan CM, Tarquinio KM, Mack EH, Fitzgerald JC,

975   Coates BM, Jackson AM, Young CC, Son MBF, Patel MM, Newburger JW, Randolph

976   AG, Overcoming COVID-19 Investigators. 2021. Characteristics and Outcomes of US

977   Children and Adolescents With Multisystem Inflammatory Syndrome in Children (MIS-C)

978   Compared With Severe Acute COVID-19. *JAMA*. doi:10.1001/jama.2021.2091

979   Flanagan KL, Fink AL, Plebanski M, Klein SL. 2017. Sex and Gender Differences in the

980   Outcomes of Vaccination over the Life Course. *Annu Rev Cell Dev Biol* **33**:577–599.

981   Gallo Marin B, Aghagoli G, Lavine K, Yang L, Siff EJ, Chiang SS, Salazar-Mather TP, Dumenco

982   L, Savaria MC, Aung SN, Flanigan T, Michelow IC. 2020. Predictors of COVID-19

983   severity: A literature review. *Rev Med Virol* e2146.

984   García M, Kokkinou E, Carrasco García A, Parrot T, Palma Medina LM, Maleki KT, Christ W,

985   Varnaitė R, Filipovic I, Ljunggren H-G, Others. 2020. Innate lymphoid cell composition

986   associates with COVID-19 disease severity. *Clinical & translational immunology*

987   **9**:e1224.

988   Giamarellos-Bourboulis EJ, Netea MG, Rovina N, Akinosoglou K, Antoniadou A, Antonakos N,

989   Damoraki G, Gkavogianni T, Adami M-E, Katsaounou P, Ntaganou M, Kyriakopoulou M,

990   Dimopoulos G, Koutsodimitropoulos I, Velissaris D, Koufargyris P, Karageorgos A,

991   Katrini K, Lekakis V, Lupse M, Kotsaki A, Renieris G, Theodoulou D, Panou V, Koukaki

992   E, Koulouris N, Gogos C, Koutsoukou A. 2020. Complex Immune Dysregulation in

993   COVID-19 Patients with Severe Respiratory Failure. *Cell Host Microbe* **27**:992-1000.e3.

994   Giefing-Kröll C, Berger P, Lepperdinger G, Grubeck-Loebenstein B. 2015. How sex and age

995   affect immune responses, susceptibility to infections, and response to vaccination. *Aging*

996   *Cell* **14**:309–321.

997   Gu Z, Eils R, Schlesner M. 2016. Complex heatmaps reveal patterns and correlations in

998   multidimensional genomic data. *Bioinformatics* **32**:2847–2849.

999   Gupta RK, Harrison EM, Ho A, Docherty AB, Knight SR, van Smeden M, Abubakar I, Lipman M,

1000   Quartagno M, Pius R, Buchan I, Carson G, Drake TM, Dunning J, Fairfield CJ, Gamble

1001   C, Green CA, Halpin S, Hardwick HE, Holden KA, Horby PW, Jackson C, Mclean KA,

1002   Merson L, Nguyen-Van-Tam JS, Norman L, Olliaro PL, Pritchard MG, Russell CD, Scott-

1003   Brown J, Shaw CA, Sheikh A, Solomon T, Sudlow C, Swann OV, Turtle L, Openshaw

1004   PJM, Baillie JK, Semple MG, Noursadeghi M, ISARIC4C Investigators. 2021.

1005   Development and validation of the ISARIC 4C Deterioration model for adults hospitalised

1006   with COVID-19: a prospective cohort study. *Lancet Respir Med*. doi:10.1016/S2213-

1007   2600(20)30559-2

1008   Hashimshony T, Senderovich N, Avital G, Klochendler A, de Leeuw Y, Anavy L, Gennert D, Li

1009   S, Livak KJ, Rozenblatt-Rosen O, Dor Y, Regev A, Yanai I. 2016. CEL-Seq2: sensitive

1010   highly-multiplexed single-cell RNA-Seq. *Genome Biol* **17**:77.

1011   He J, Guo Y, Mao R, Zhang J. 2021. Proportion of asymptomatic coronavirus disease 2019: A

1012   systematic review and meta-analysis. *J Med Virol* **93**:820–830.

1013   Heald-Sargent T, Muller WJ, Zheng X, Rippe J, Patel AB, Kociolek LK. 2020. Age-Related

1014   Differences in Nasopharyngeal Severe Acute Respiratory Syndrome Coronavirus 2

1015   (SARS-CoV-2) Levels in Patients With Mild to Moderate Coronavirus Disease 2019

1016   (COVID-19). *JAMA Pediatr* **174**:902–903.

1017   Huang C, Wang Y, Li X, Ren L, Zhao J, Hu Y, Zhang L, Fan G, Xu J, Gu X, Cheng Z, Yu T, Xia

1018   J, Wei Y, Wu W, Xie X, Yin W, Li H, Liu M, Xiao Y, Gao H, Guo L, Xie J, Wang G, Jiang

1019   R, Gao Z, Jin Q, Wang J, Cao B. 2020. Clinical features of patients infected with 2019

1020   novel coronavirus in Wuhan, China. *Lancet* **395**:497–506.

1021 Huang I, Pranata R. 2020. Lymphopenia in severe coronavirus disease-2019 (COVID-19):

1022   systematic review and meta-analysis. *J Intensive Care Med* **8**:36.

1023 Jamieson AM, Pasman L, Yu S, Gamradt P, Homer RJ, Decker T, Medzhitov R. 2013. Role of

1024   tissue protection in lethal respiratory viral-bacterial coinfection. *Science* **340**:1230–1234.

1025 Jhaveri KA, Trammell RA, Toth LA. 2007. Effect of environmental temperature on sleep,

1026   locomotor activity, core body temperature and immune responses of C57BL/6J mice.

1027   *Brain Behav Immun* **21**:975–987.

1028 Jones TC, Biele G, Mühlemann B, Veith T, Schneider J, Beheim-Schwarzbach J, Bleicker T,

1029   Tesch J, Schmidt ML, Sander LE, Kurth F, Menzel P, Schwarzer R, Zuchowski M,

1030   Hofmann J, Krumbholz A, Stein A, Edelmann A, Corman VM, Drosten C. 2021.

1031   Estimating infectiousness throughout SARS-CoV-2 infection course. *Science*

1032   **373**:eabi5273.

1033 Kaneko N, Kuo H-H, Boucau J, Farmer JR, Allard-Chamard H, Mahajan VS, Piechocka-Trocha

1034   A, Lefteri K, Osborn M, Bals J, Bartsch YC, Bonheur N, Caradonna TM, Chevalier J,

1035   Chowdhury F, Diefenbach TJ, Einkauf K, Fallon J, Feldman J, Finn KK, Garcia-

1036   Broncano P, Hartana CA, Hauser BM, Jiang C, Kaplonek P, Karpell M, Koscher EC,

1037   Lian X, Liu H, Liu J, Ly NL, Michell AR, Rassadkina Y, Seiger K, Sessa L, Shin S, Singh

1038   N, Sun W, Sun X, Ticheli HJ, Waring MT, Zhu AL, Alter G, Li JZ, Lingwood D, Schmidt

1039   AG, Lichterfeld M, Walker BD, Yu XG, Padera RF Jr, Pillai S, Massachusetts

1040   Consortium on Pathogen Readiness Specimen Working Group. 2020. Loss of Bcl-6-

1041   Expressing T Follicular Helper Cells and Germinal Centers in COVID-19. *Cell*.

1042   doi:10.1016/j.cell.2020.08.025

1043 Karlberg J. 2004. Do Men Have a Higher Case Fatality Rate of Severe Acute Respiratory

1044   Syndrome than Women Do? *American Journal of Epidemiology*. doi:10.1093/aje/kwh056

1045 Kassambara A. 2020. ggpubr: "ggplot2" Based Publication Ready Plots.

1046 Klein SL, Flanagan KL. 2016. Sex differences in immune responses. *Nat Rev Immunol* **16**:626–

1047   638.

1048 Klose CSN, Artis D. 2016. Innate lymphoid cells as regulators of immunity, inflammation and

1049   tissue homeostasis. *Nat Immunol* **17**:765–774.

1050 Kløverpris HN, Kazer SW, Mjösberg J, Mabuka JM, Wellmann A, Ndhlovu Z, Yadon MC,

1051   Nhamoyebonde S, Muenchhoff M, Simoni Y, Andersson F, Kuhn W, Garrett N, Burgers

1052   WA, Kamya P, Pretorius K, Dong K, Moodley A, Newell EW, Kasprowicz V, Abdool

1053   Karim SS, Goulder P, Shalek AK, Walker BD, Ndung'u T, Leslie A. 2016. Innate

1054   Lymphoid Cells Are Depleted Irreversibly during Acute HIV-1 Infection in the Absence of

1055   Viral Suppression. *Immunity* **44**:391–405.

1056 Kompaniyets L. 2021. Body Mass Index and Risk for COVID-19–Related Hospitalization,

1057   Intensive Care Unit Admission, Invasive Mechanical Ventilation, and Death — United

1058   States, March–December 2020. *MMWR Morb Mortal Wkly Rep* **70**.

1059   doi:10.15585/mmwr.mm7010e4

1060 Kuri-Cervantes L, Pampena MB, Meng W, Rosenfeld AM, Ittner CAG, Weisman AR, Agyekum

1061   RS, Mathew D, Baxter AE, Vella LA, Kuthuru O, Apostolidis SA, Bershaw L, Dougherty

1062   J, Greenplate AR, Pattekar A, Kim J, Han N, Gouma S, Weirick ME, Arevalo CP, Bolton

1063   MJ, Goodwin EC, Anderson EM, Hensley SE, Jones TK, Mangalmurti NS, Luning Prak

1064   ET, Wherry EJ, Meyer NJ, Betts MR. 2020. Comprehensive mapping of immune

1065   perturbations associated with severe COVID-19. *Sci Immunol* **5**:eabd7114.

1066 Kuznetsova A, Brockhoff PB, Christensen RHB, Others. 2017. lmerTest package: tests in linear

1067   mixed effects models. *J Stat Softw* **82**:1–26.

1068 Laxminarayan R, Wahl B, Dudala SR, Gopal K, Mohan B C, Neelima S, Jawahar Reddy KS,

1069   Radhakrishnan J, Lewnard JA. 2020. Epidemiology and transmission dynamics of

1070   COVID-19 in two Indian states. *Science* **370**:691–697.

1071 Lee S, Kim T, Lee E, Lee C, Kim H, Rhee H, Park SY, Son H-J, Yu S, Park JW, Choo EJ, Park

1072   S, Loeb M, Kim TH. 2020. Clinical Course and Molecular Viral Shedding Among

1073   Asymptomatic and Symptomatic Patients With SARS-CoV-2 Infection in a Community

1074   Treatment Center in the Republic of Korea. *JAMA Internal Medicine* **180**:1447.

1075 Leist SR, Dinnon KH 3rd, Schäfer A, Tse LV, Okuda K, Hou YJ, West A, Edwards CE, Sanders

1076   W, Fritch EJ, Gully KL, Scobey T, Brown AJ, Sheahan TP, Moorman NJ, Boucher RC,

1077   Gralinski LE, Montgomery SA, Baric RS. 2020. A Mouse-Adapted SARS-CoV-2 Induces

1078   Acute Lung Injury and Mortality in Standard Laboratory Mice. *Cell* **183**:1070-1085.e12.

1079 Lennon NJ, Bhattacharyya RP, Mina MJ, Rehm HL, Hung DT, Smole S, Woolley A, Lander ES,

1080   Gabriel SB. 2021. Cross-sectional assessment of SARS-CoV-2 viral load by symptom

1081   status in Massachusetts congregate living facilities. *J Infect Dis*.

1082   doi:10.1093/infdis/jiab367

1083 Lennon NJ, Bhattacharyya RP, Mina MJ, Rehm HL, Hung DT, Smole S, Woolley A, Lander ES,

1084   Gabriel SB. 2020. Comparison of viral levels in individuals with or without symptoms at

1085   time of COVID-19 testing among 32,480 residents and staff of nursing homes and

1086   assisted living facilities in Massachusetts. *bioRxiv*. doi:10.1101/2020.07.20.20157792

1087 Lenth R. 2020. emmeans: Estimated Marginal Means, aka Least-Squares Means.

1088 Li B, Dewey CN. 2011. RSEM: accurate transcript quantification from RNA-Seq data with or

1089   without a reference genome. *BMC Bioinformatics* **12**:323.

1090 Li B, Zhang S, Zhang R, Chen X, Wang Y, Zhu C. 2020. Epidemiological and Clinical

1091   Characteristics of COVID-19 in Children: A Systematic Review and Meta-Analysis. *Front*

1092   *Pediatr* **8**:591132.

1093 Licciardi F, Pruccoli G, Denina M, Parodi E, Taglietto M, Rosati S, Montin D. 2020. SARS-CoV-

1094   2-Induced Kawasaki-Like Hyperinflammatory Syndrome: A Novel COVID Phenotype in

1095   Children. *Pediatrics*. doi:10.1542/peds.2020-1711

1096 López-Otín C, Kroemer G. 2021. Hallmarks of Health. *Cell* **184**:33–63.

1097 LoTempio JE, Billings EA, Draper K, Ralph C, Moshgriz M, Duong N, Bard JD, Gai X, Wessel D,

1098   DeBiasi RL, Campos JM, Vilain E, Delaney M, Michael DG. 2021. Novel SARS-CoV-2

1099   spike variant identified through viral genome sequencing of the pediatric Washington

1100   D.C. COVID-19 outbreak. *medRxiv* 2021.02.08.21251344.

1101   Love M, Anders S, Huber W. 2014. Differential analysis of count data--the DESeq2 package.

1102   *Genome Biol* **15**:550.

1103   Lu X, Zhang L, Du H, Zhang J, Li YY, Qu J, Zhang W, Wang Y, Bao S, Li Y, Wu C, Liu H, Liu D,

1104   Shao J, Peng X, Yang Y, Liu Z, Xiang Y, Zhang F, Silva RM, Pinkerton KE, Shen K, Xiao

1105   H, Xu S, Wong GWK, Chinese Pediatric Novel Coronavirus Study Team. 2020. SARS-

1106   CoV-2 Infection in Children. *N Engl J Med* **382**:1663–1665.

1107   Lucas C, Wong P, Klein J, Castro TBR, Silva J, Sundaram M, Ellingson MK, Mao T, Oh JE,

1108   Israelow B, Takahashi T, Tokuyama M, Lu P, Venkataraman A, Park A, Mohanty S,

1109   Wang H, Wyllie AL, Vogels CBF, Earnest R, Lapidus S, Ott IM, Moore AJ, Muenker MC,

1110   Fournier JB, Campbell M, Odio CD, Casanovas-Massana A, Yale IMPACT Team,

1111   Herbst R, Shaw AC, Medzhitov R, Schulz WL, Grubaugh ND, Dela Cruz C, Farhadian S,

1112   Ko AI, Omer SB, Iwasaki A. 2020. Longitudinal analyses reveal immunological misfiring

1113   in severe COVID-19. *Nature* **584**:463–469.

1114   Luo X, Zhou W, Yan X, Guo T, Wang B, Xia H, Ye L, Xiong J, Jiang Z, Liu Y, Zhang B, Yang W.

1115   2020. Prognostic Value of C-Reactive Protein in Patients With Coronavirus 2019. *Clin*

1116   *Infect Dis* **71**:2174–2179.

1117   Márquez EJ, Chung C-H, Marches R, Rossi RJ, Nehar-Belaid D, Eroglu A, Mellert DJ, Kuchel

1118   GA, Banchereau J, Ucar D. 2020. Sexual-dimorphism in human immune system aging.

1119   *Nat Commun* **11**:751.

1120   Mathew D, Giles JR, Baxter AE, Oldridge DA, Greenplate AR, Wu JE, Alanio C, Kuri-Cervantes

1121   L, Pampena MB, D'Andrea K, Manne S, Chen Z, Huang YJ, Reilly JP, Weisman AR,

1122   Ittner CAG, Kuthuru O, Dougherty J, Nzingha K, Han N, Kim J, Pattekar A, Goodwin EC,

1123   Anderson EM, Weirick ME, Gouma S, Arevalo CP, Bolton MJ, Chen F, Lacey SF,

1124   Ramage H, Cherry S, Hensley SE, Apostolidis SA, Huang AC, Vella LA, UPenn COVID

1125   Processing Unit, Betts MR, Meyer NJ, Wherry EJ. 2020. Deep immune profiling of

1126   COVID-19 patients reveals distinct immunotypes with therapeutic implications. *Science*

1127   **369**. doi:10.1126/science.abc8511

1128   Mauvais-Jarvis F. 2020. Aging, Male Sex, Obesity, and Metabolic Inflammation Create the

1129   Perfect Storm for COVID-19. *Diabetes* **69**:1857–1863.

1130   McCarville JL, Ayres JS. 2018. Disease tolerance: concept and mechanisms. *Curr Opin*

1131   *Immunol* **50**:88–93.

1132   Medzhitov R, Schneider DS, Soares MP. 2012. Disease tolerance as a defense strategy.

1133   *Science* **335**:936–941.

1134   Monticelli LA, Osborne LC, Noti M, Tran SV, Zaiss DMW, Artis D. 2015. IL-33 promotes an

1135   innate immune pathway of intestinal tissue protection dependent on amphiregulin–EGFR

1136   interactions. *Proc Natl Acad Sci U S A* **112**:10762–10767.

1137   Monticelli LA, Sonnenberg GF, Abt MC, Alenghat T, Ziegler CGK, Doering TA, Angelosanto JM,

1138   Laidlaw BJ, Yang CY, Sathaliyawala T, Kubota M, Turner D, Diamond JM, Goldrath AW,

1139   Farber DL, Collman RG, Wherry EJ, Artis D. 2011. Innate lymphoid cells promote lung-

1140   tissue homeostasis after infection with influenza virus. *Nat Immunol* **12**:1045–1054.

1141   Mudd PA, Crawford JC, Turner JS, Souquette A, Reynolds D, Bender D, Bosanquet JP, Anand

1142   NJ, Striker DA, Martin RS, Boon ACM, House SL, Remy KE, Hotchkiss RS, Presti RM,

1143   O'Halloran JA, Powderly WG, Thomas PG, Ellebedy AH. 2020. Distinct inflammatory

1144   profiles distinguish COVID-19 from influenza with limited contributions from cytokine

1145   storm. *Sci Adv* **6**. doi:10.1126/sciadv.abe3024

1146   O'Driscoll M, Ribeiro Dos Santos G, Wang L, Cummings DAT, Azman AS, Paireau J, Fontanet

1147   A, Cauchemez S, Salje H. 2020. Age-specific mortality and immunity patterns of SARS-

1148   CoV-2. *Nature*. doi:10.1038/s41586-020-2918-0

1149   Patin E, Hasan M, Bergstedt J, Rouilly V, Libri V, Urrutia A, Alanio C, Scepanovic P, Hammer C,

1150   Jönsson F, Beitz B, Quach H, Lim YW, Hunkapiller J, Zepeda M, Green C, Piasecka B,

1151   Leloup C, Rogge L, Huetz F, Peguillet I, Lantz O, Fontes M, Di Santo JP, Thomas S,

1152   Fellay J, Duffy D, Quintana-Murci L, Albert ML, Milieu Intérieur Consortium. 2018.

1153   Natural variation in the parameters of innate immune cells is preferentially driven by

1154   genetic factors. *Nat Immunol* **19**:302–314.

1155   Peckham H, de Gruijter NM, Raine C, Radziszewska A, Ciurtin C, Wedderburn LR, Rosser EC,

1156   Webb K, Deakin CT. 2020. Male sex identified by global COVID-19 meta-analysis as a

1157   risk factor for death and ITU admission. *Nature Communications* **11**:6317.

1158   Petrilli CM, Jones SA, Yang J, Rajagopalan H, O'Donnell L, Chernyak Y, Tobin KA, Cerfolio RJ,

1159   Francois F, Horwitz LI. 2020. Factors associated with hospital admission and critical

1160   illness among 5279 people with coronavirus disease 2019 in New York City: prospective

1161   cohort study. *BMJ* **369**:m1966.

1162   Piasecka B, Duffy D, Urrutia A, Quach H, Patin E, Posseme C, Bergstedt J, Charbit B, Rouilly V,

1163   MacPherson CR, Hasan M, Albaud B, Gentien D, Fellay J, Albert ML, Quintana-Murci L,

1164   Milieu Intérieur Consortium. 2018. Distinctive roles of age, sex, and genetics in shaping

1165   transcriptional variation of human immune responses to microbial challenges. *Proc Natl*

1166   *Acad Sci U S A* **115**:E488–E497.

1167   Poline J, Gaschignard J, Leblanc C, Madhi F, Foucaud E, Nattes E, Faye A, Bonacorsi S,

1168   Mariani P, Varon E, Smati-Lafarge M, Caseris M, Basmaci R, Lachaume N, Ouldali N.

1169   2020. Systematic SARS-CoV-2 screening at hospital admission in children:a French

1170   prospective multicenter study. *Clin Infect Dis*. doi:10.1093/cid/ciaa1044

1171   R Core Team. 2020. R: A Language and Environment for Statistical Computing.

1172   Ra SH, Lim JS, Kim G-U, Kim MJ, Jung J, Kim S-H. 2021. Upper respiratory viral load in

1173   asymptomatic individuals and mildly symptomatic patients with SARS-CoV-2 infection.

1174   *Thorax* **76**:61–63.

1175   Råberg L, Sim D, Read AF. 2007. Disentangling genetic variation for resistance and tolerance

1176   to infectious diseases in animals. *Science* **318**:812–814.

1177   Rak GD, Osborne LC, Siracusa MC, Kim BS, Wang K, Bayat A, Artis D, Volk SW. 2016. IL-33-

1178   Dependent Group 2 Innate Lymphoid Cells Promote Cutaneous Wound Healing. *J Invest*

1179   *Dermatol* **136**:487–496.

1180   Rauber S, Luber M, Weber S, Maul L, Soare A, Wohlfahrt T, Lin N-Y, Dietel K, Bozec A,

1181   Herrmann M, Kaplan MH, Weigmann B, Zaiss MM, Fearon U, Veale DJ, Cañete JD,

1182   Distler O, Rivellese F, Pitzalis C, Neurath MF, McKenzie ANJ, Wirtz S, Schett G, Distler

1183   JHW, Ramming A. 2017. Resolution of inflammation by interleukin-9-producing type 2

1184   innate lymphoid cells. *Nat Med* **23**:938–944.

1185   Richardson S, Hirsch JS, Narasimhan M, Crawford JM, McGinn T, Davidson KW, the Northwell

1186   COVID-19 Research Consortium, Barnaby DP, Becker LB, Chelico JD, Cohen SL,

1187   Cookingham J, Coppa K, Diefenbach MA, Dominello AJ, Duer-Hefele J, Falzon L, Gitlin

1188   J, Hajizadeh N, Harvin TG, Hirschwerk DA, Kim EJ, Kozel ZM, Marrast LM, Mogavero

1189   JN, Osorio GA, Qiu M, Zanos TP. 2020. Presenting Characteristics, Comorbidities, and

1190   Outcomes Among 5700 Patients Hospitalized With COVID-19 in the New York City

1191   Area. *JAMA* **323**:2052–2059.

1192   Riphagen S, Gomez X, Gonzalez-Martinez C, Wilkinson N, Theocharis P. 2020.

1193   Hyperinflammatory shock in children during COVID-19 pandemic. *Lancet*.

1194   Sanchez KK, Chen GY, Schieber AMP, Redford SE, Shokhirev MN, Leblanc M, Lee YM, Ayres

1195   JS. 2018. Cooperative Metabolic Adaptations in the Host Can Favor Asymptomatic

1196   Infection and Select for Attenuated Virulence in an Enteric Pathogen. *Cell* **175**:146-

1197   158.e15.

1198   Sancho-Shimizu V, Brodin P, Cobat A, Biggs CM, Toubiana J, Lucas CL, Henrickson SE, Belot

1199   A, MIS-C@CHGE, Tangye SG, Milner JD, Levin M, Abel L, Bogunovic D, Casanova J-L,

1200   Zhang S-Y. 2021. SARS-CoV-2–related MIS-C: A key to the viral and genetic causes of

1201   Kawasaki disease? *J Exp Med* **218**. doi:10.1084/jem.20210446

1202   Schneider DS, Ayres JS. 2008. Two ways to survive infection: what resistance and tolerance

1203   can teach us about treating infectious diseases. *Nature Reviews Immunology* **8**:889–

1204   895.

1205   Scully EP, Haverfield J, Ursin RL, Tannenbaum C, Klein SL. 2020. Considering how biological

1206   sex impacts immune responses and COVID-19 outcomes. *Nat Rev Immunol* **20**:442–

1207   447.

1208   Solana R, Tarazona R, Gayoso I, Lesur O, Dupuis G, Fulop T. 2012. Innate

1209   immunosenescence: effect of aging on cells and receptors of the innate immune system

1210   in humans. *Semin Immunol* **24**:331–341.

1211   Tesoriero JM, Swain C-AE, Pierce JL, Zamboni L, Wu M, Holtgrave DR, Gonzalez CJ, Udo T,

1212   Morne JE, Hart-Malloy R, Rajulu DT, Leung S-YJ, Rosenberg ES. 2021. COVID-19

1213   Outcomes Among Persons Living With or Without Diagnosed HIV Infection in New York

1214   State. *JAMA Netw Open* **4**:e2037069.

1215   Verdoni L, Mazza A, Gervasoni A, Martelli L, Ruggeri M, Ciuffreda M, Bonanomi E, D'Antiga L.

1216   2020. An outbreak of severe Kawasaki-like disease at the Italian epicentre of the SARS-

1217   CoV-2 epidemic: an observational cohort study. *Lancet* **395**:1771–1778.

1218   Vivier E, Artis D, Colonna M, Diefenbach A, Di Santo JP, Eberl G, Koyasu S, Locksley RM,

1219   McKenzie ANJ, Mebius RE, Powrie F, Spits H. 2018. Innate Lymphoid Cells: 10 Years

1220   On. *Cell* **174**:1054–1066.

1221   Wang A, Huen SC, Luan HH, Yu S, Zhang C, Gallezot J-D, Booth CJ, Medzhitov R. 2016.

1222   Opposing Effects of Fasting Metabolism on Tissue Tolerance in Bacterial and Viral

1223   Inflammation. *Cell* **166**:1512-1525.e12.

1224   Wang Y, Lifshitz L, Gellatly K, Vinton CL, Busman-Sahay K, McCauley S, Vangala P, Kim K,

1225   Derr A, Jaiswal S, Kucukural A, McDonel P, Hunt PW, Greenough T, Houghton J,

1226   Somsouk M, Estes JD, Brenchley JM, Garber M, Deeks SG, Luban J. 2020. HIV-1-

1227   induced cytokines deplete homeostatic innate lymphoid cells and expand TCF7-

1228   dependent memory NK cells. *Nat Immunol* **21**:274–286.

1229   Whittaker E, Bamford A, Kenny J, Kaforou M, Jones CE, Shah P, Ramnarayan P, Fraisse A,

1230   Miller O, Davies P, Kucera F, Brierley J, McDougall M, Carter M, Tremoulet A, Shimizu

1231   C, Herberg J, Burns JC, Lyall H, Levin M, PIMS-TS Study Group and EUCLIDS and

1232   PERFORM Consortia. 2020. Clinical Characteristics of 58 Children With a Pediatric

1233   Inflammatory Multisystem Syndrome Temporally Associated With SARS-CoV-2. *JAMA*

1234   **324**:259–269.

1235   Wickham H. 2016. ggplot2: Elegant Graphics for Data Analysis. Springer.

1236   Wickham H, Averick M, Bryan J, Chang W, McGowan L, François R, Grolemund G, Hayes A,

1237   Henry L, Hester J, Kuhn M, Pedersen T, Miller E, Bache S, Müller K, Ooms J, Robinson

1238   D, Seidel D, Spinu V, Takahashi K, Vaughan D, Wilke C, Woo K, Yutani H. 2019.

1239   Welcome to the Tidyverse. *JOSS* **4**:1686.

1240   Yang Q, Monticelli LA, Saenz SA, Chi AW-S, Sonnenberg GF, Tang J, De Obaldia ME, Bailis

1241   W, Bryson JL, Toscano K, Huang J, Haczku A, Pear WS, Artis D, Bhandoola A. 2013. T

1242   cell factor 1 is required for group 2 innate lymphoid cell generation. *Immunity* **38**:694–

1243   704.

1244   Yang Q, Saldi TK, Gonzales PK, Lasda E, Decker CJ, Tat KL, Fink MR, Hager CR, Davis JC,

1245   Ozeroff CD, Muhlrad D, Clark SK, Fattor WT, Meyerson NR, Paige CL, Gilchrist AR,

1246   Barbachano-Guerrero A, Worden-Sapper ER, Wu SS, Brisson GR, McQueen MB,

1247   Dowell RD, Leinwand L, Parker R, Sawyer SL. 2021. Just 2% of SARS-CoV-2−positive

1248   individuals carry 90% of the virus circulating in communities. *Proc Natl Acad Sci U S A*

1249   **118**. doi:10.1073/pnas.2104547118

1250   Yonker LM, Gilboa T, Ogata AF, Senussi Y, Lazarovits R, Boribong BP, Bartsch YC, Loiselle M,

1251   Noval Rivas M, Porritt RA, Lima R, Davis JP, Farkas EJ, Burns MD, Young N, Mahajan

1252   VS, Hajizadeh S, Herrera Lopez XI, Kreuzer J, Morris R, Martinez EE, Han I, Griswold K

1253   Jr, Barry NC, Thompson DB, Church G, Edlow AG, Haas W, Pillai S, Arditi M, Alter G,

1254   Walt DR, Fasano A. 2021. Multisystem inflammatory syndrome in children is driven by

1255   zonulin-dependent loss of gut mucosal barrier. *J Clin Invest*. doi:10.1172/JCI149633

1256   Yonker LM, Neilan AM, Bartsch Y, Patel AB, Regan J, Arya P, Gootkind E, Park G, Hardcastle

1257   M, St John A, Appleman L, Chiu ML, Fialkowski A, De la Flor D, Lima R, Bordt EA,

1258   Yockey LJ, D'Avino P, Fischinger S, Shui JE, Lerou PH, Bonventre JV, Yu XG, Ryan ET,

1259   Bassett IV, Irimia D, Edlow AG, Alter G, Li JZ, Fasano A. 2020. Pediatric Severe Acute

1260   Respiratory Syndrome Coronavirus 2 (SARS-CoV-2): Clinical Presentation, Infectivity,

1261   and Immune Responses. *J Pediatr* **227**:45-52.e5.

1262   Yu G, Wang L-G, Han Y, He Q-Y. 2012. clusterProfiler: an R Package for Comparing Biological

1263   Themes Among Gene Clusters. *OMICS* **16**:284–287.

1264   Yudanin NA, Schmitz F, Flamar A-L, Thome JJC, Tait Wojno E, Moeller JB, Schirmer M, Latorre

1265   IJ, Xavier RJ, Farber DL, Monticelli LA, Artis D. 2019. Spatial and Temporal Mapping of

1266   Human Innate Lymphoid Cells Reveals Elements of Tissue Specificity. *Immunity* **50**:505-

1267   519.e4.

1268   Yukselen O, Turkyilmaz O, Ozturk AR, Garber M, Kucukural A. 2020. DolphinNext: a distributed

1269   data processing platform for high throughput genomics. *BMC Genomics* **21**:310.

1270   Zhang Z-L, Hou Y-L, Li D-T, Li F-Z. 2020. Laboratory findings of COVID-19: a systematic review

1271   and meta-analysis. *Scand J Clin Lab Invest* **80**:441–447.

1272   Zhao Q, Meng M, Kumar R, Wu Y, Huang J, Deng Y, Weng Z, Yang L. 2020. Lymphopenia is

1273   associated with severe coronavirus disease 2019 (COVID-19) infections: A systemic

1274   review and meta-analysis. *Int J Infect Dis* **96**:131–135.

1275   Zheng M, Gao Y, Wang G, Song G, Liu S, Sun D, Xu Y, Tian Z. 2020. Functional exhaustion of

1276   antiviral lymphocytes in COVID-19 patients. *Cell Mol Immunol*.

1277   Zhou F, Yu T, Du R, Fan G, Liu Y, Liu Z, Xiang J, Wang Y, Song B, Gu X, Guan L, Wei Y, Li H,

1278   Wu X, Xu J, Tu S, Zhang Y, Chen H, Cao B. 2020. Clinical course and risk factors for

1279   mortality of adult inpatients with COVID-19 in Wuhan, China: a retrospective cohort

1280   study. *Lancet* **395**:1054–1062.

1281

1282

1283

Source data file legends, supplementary table legends, and figure supplements with legends

Source Data files:

Figure 2 - Source data 1: Combined demographic, clinical, and flow cytometry data for adult COVID-19 and control cohorts. Data included in this file are associated with Figures 1-3; Figure 3–figure supplement 1; Figure 6; tables 1-4; and supplementary tables S3-S4. File name: Adult_COVIDandControl_data.xlsx

Figure 4 - Source data 1: Combined demographic, clinical, and flow cytometry data for pediatric COVID-19, MIS-C, and control cohorts. Data included in this file are associated with Figures 1 and 4; Figure 4–figure supplement 1; Figure 4–figure supplement 2; table 5, and supplementary tables S2, S5, and S6. File name: Pediatric_ COVID_MISC_andControl_data.xlsx

Figure 6 - Source data 1: Amphiregulin (AREG) flow cytometry data presented in Figure 6 and Figure 6-figure supplement 1. File name: AREG_in_ILCs.xlsx

Supplementary file tables:

Supplementary file 1:

- **Supplementary file 1a:** Antibodies Used in Flow Cytometry

- **Supplementary file 1b:** Primers for bulk RNA-Seq

1372

1373

1374

1375

1376

1377

1378

1379
1380

Figure supplements:

A

B

C

D

E
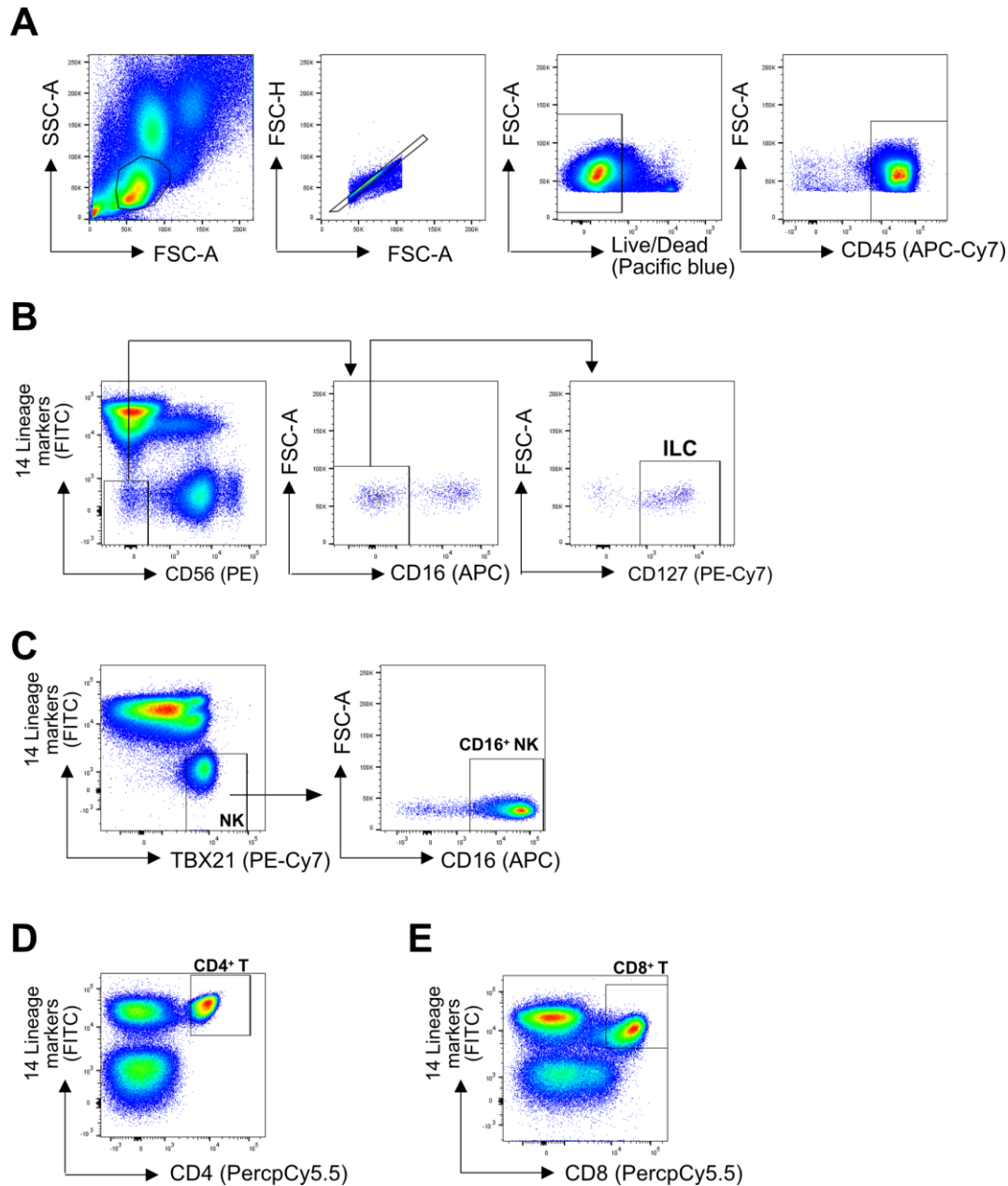
1382

1383
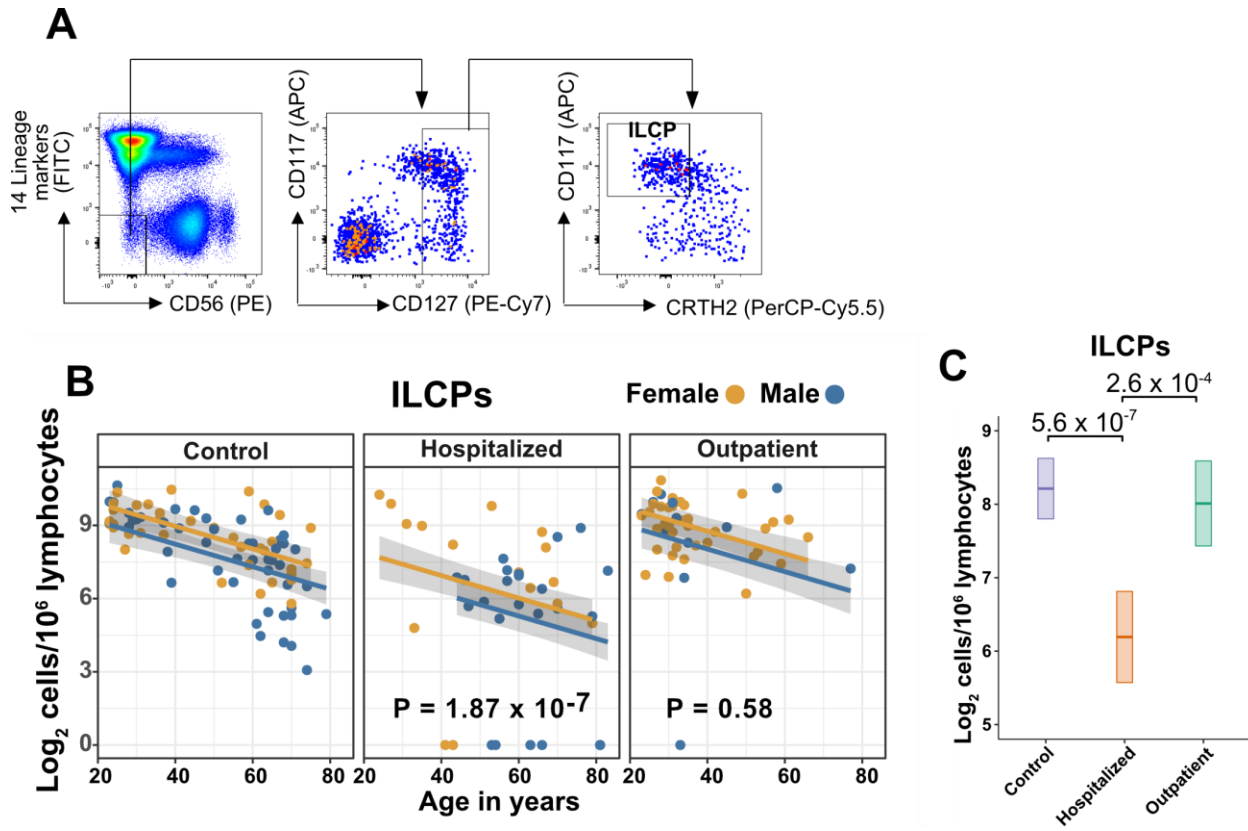
Figure 2–figure supplement 1. Representative gating strategy

(A) All cell subsets were first gated on lymphoid cells, singlets, live/dead, and CD45$^+$. Lineage (Lin) markers included antibodies against: CD3, CD4, TCRαβ, TCRγδ, CD19, CD20, CD22, CD34, FcεRIα, CD11c, CD303, CD123, CD1a, and CD14.

(B) ILCs were identified as Lin$^-$CD56$^-$CD16$^-$CD127$^+$

(C) CD16$^+$ NK cells were identified as Lin$^-$TBX21$^+$CD16$^+$

(E) CD4$^+$ T cells were identified as Lin$^+$CD4$^+$ (D), and CD8$^+$ T cells were identified as Lin$^+$CD8$^+$

A

B

C

Figure 3–figure supplement 1. Innate lymphoid cell precursors (ILCPs) decrease with age and are depleted in patients hospitalized with COVID-19

(A) Representative gating for ILCP identification in PBMCs. Cells were first gated on lymphoid cells, singlets, live/dead, and CD45$^+$. Lineage (Lin) markers included antibodies against: CD3, CD4, TCRαβ, TCRγδ, CD19, CD20, CD22, CD34, FcεRIα, CD11c, CD303, CD123, CD1a, and CD14.

(B) Effect of age (X-axis) on log$_2$ ILCP abundance per million total lymphocytes (Y-axis). Each dot represents an individual blood donor, with yellow for female and blue for male. Shading represents the 95%CI. P-values are from the regression analysis for comparisons to the control group.

(C) Lymphoid cell abundance by group, shown as estimated marginal means with 95%CI, generated from the multiple linear regressions in (B), and averaged across age and sex. P-values represent pairwise comparisons on the estimated marginal means, adjusted for multiple comparisons with the Tukey method.

1414

A
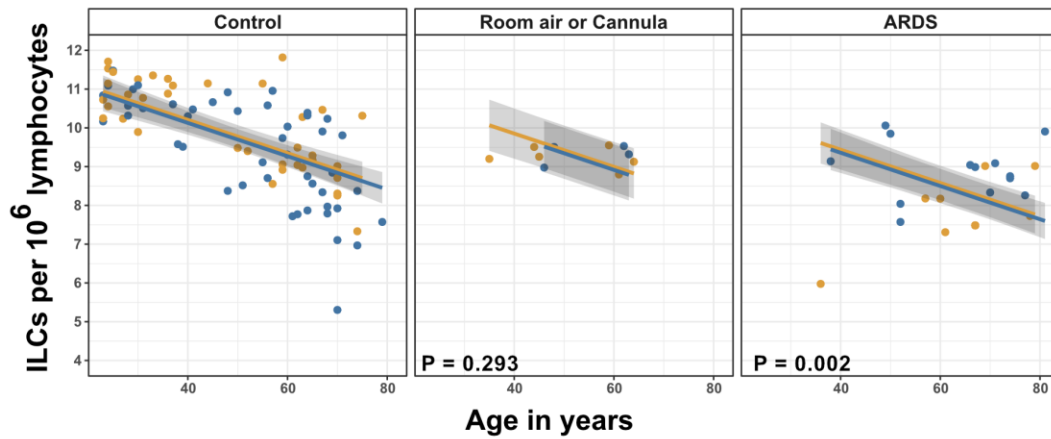
B

Group differences in ILC[a] abundance adjusted for age and sex

Group	Fold difference (log2) [±95%CI]
On room air or nasal cannula	-0.353 [-1.016, 0.309]
ARDS	-0.769** [-1.250, -0.288]

* p < 0.05, ** p < 0.01, *** p < 0.001
[a]per 10^6 lymphocytes

1415
1416

1417 **Figure 3–figure supplement 2. Association of blood ILC depletion with COVID-19**
1418 **severity in an independent cohort of adults.**
1419 (A) Effect of age (X-axis) on $\log_2$ ILC abundance per million total lymphocytes (Y-axis) in
1420 adult controls from this paper and patients with COVID-19 from Kuri-Cervantes et al.,
1421 2020. Patients were stratified into two groups by disease severity. The first group included
1422 patients maintained on room air or treated with O2 by nasal cannula. The second group
1423 included those with ARDS. Each dot represents an individual blood donor, with yellow for
1424 female and blue for male. Shading represents the 95%CI. P-values are from the
1425 regression analysis for comparisons to the control group.
1426 (C) Table of regression coefficients for $\log_2$ fold difference in ILC abundance for patients
1427 with COVID-19, in comparison to the adult healthy control cohort, adjusted for effects of
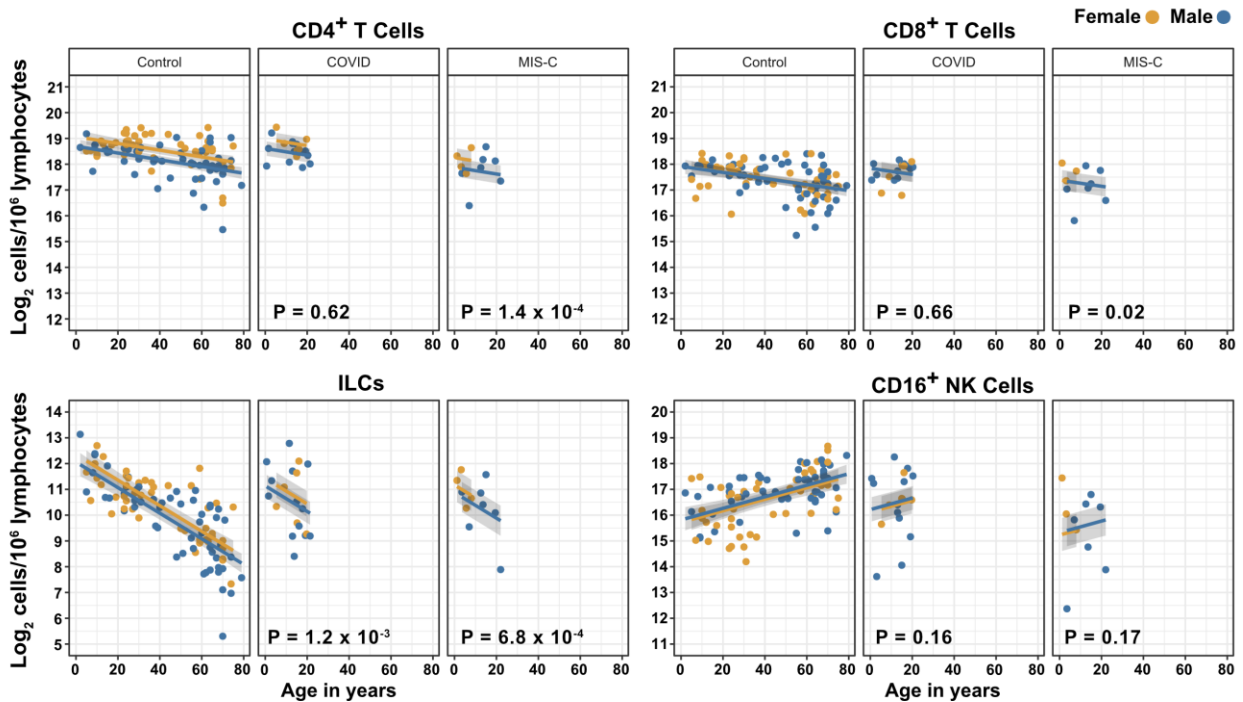1428 age and sex.

1429
1430
1431

1432

1433

1434

Figure 4–figure supplement 1. Effects of pediatric COVID-19 and MIS-C on blood lymphoid cell subsets in comparison to full combined adult and pediatric control group

Effect of age (X-axis) on $\log_2$ abundance per million total lymphocytes of the indicated lymphoid cell populations (Y-axis). Each dot represents an individual blood donor, with yellow for female and blue for male. Shading represents the 95%CI. P-values are from the regression analysis for comparisons to the control group.

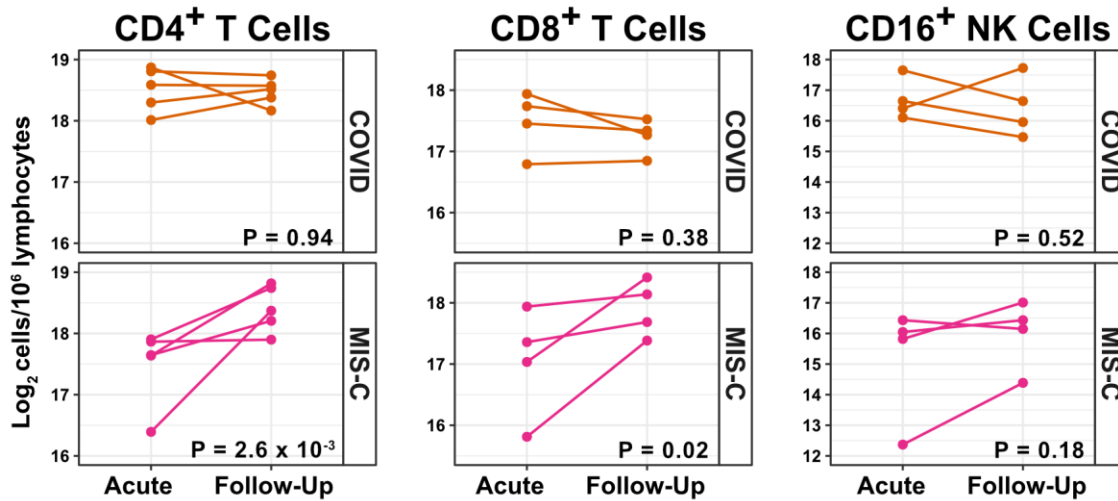1442
1443
1444
1445
1446
1447
1448
1449
1450
1451
1452
1453
1454
1455
1456
1457

1458

1459
1460

Figure 4–figure supplement 2. T cells increase during follow-up from MIS-C
Log_2 ILC abundance per million lymphocytes in longitudinal pairs of samples collected during acute presentation and during follow-up, from individual children with COVID-19 or MIS-C. P-values are for change in ILC abundance at follow-up, as determined with a linear mixed model, adjusting for age, sex, and group, and with patient as a random effect. Differences in sample size among cell types was due to limited sample availability.
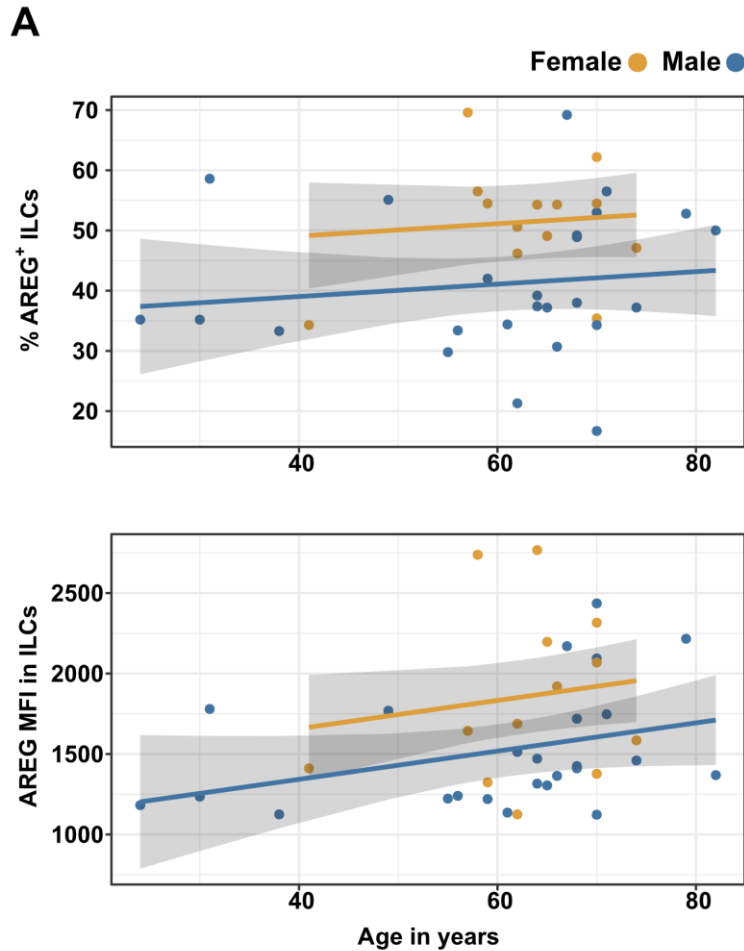
1467
1468
1469
1470
1471
1472
1473
1474
1475
1476
1477
1478
1479
1480
1481
1482

A

B

Difference [±95%CI]		
	% AREG+	**MFI in ILCs**
Age	0.103	8.764
	[-0.190, 0.397]	[-2.033, 19.561]
Male	-10.030*	-314.816*
	[-18.037, -2.023]	[-609.660, -19.973]
R^2	0.174	0.189

* p < 0.05, ** p < 0.01, *** p < 0.001

1483
1484
1485 **Figure 6–figure supplement 1. Males have lower percent AREG+ ILCs, and lower**
1486 **AREG MFI in ILCs, than do females, and there is no effect of age on these**
1487 **parameters**
1488 (A) Effect of age (X-axis) on % AREG+ ILCs or MFI in ILCs (Y-axis as indicated). Each
1489 dot represents an individual blood donor, with yellow for female and blue for male.
1490 Shading represents the 95%CI.
1491 (B) Table of results for regression analyses plotted in (A)